Karyopherins regulate nuclear pore complex barrier and transport function

Larisa E. Kapinos,* Binlu Huang,* Chantal Rencurel, and Roderick Y.H. Lim

Biozentrum and the Swiss Nanoscience Institute, University of Basel, Basel, Switzerland

Nucleocytoplasmic transport is sustained by karyopherins (Kaps) and a Ran guanosine triphosphate (RanGTP) gradient that imports nuclear localization signal (NLS)–specific cargoes (NLS-cargoes) into the nucleus. However, how nuclear pore complex (NPC) barrier selectivity, Kap traffic, and NLS-cargo release are systematically linked and simultaneously regulated remains incoherent. In this study, we show that Kapα facilitates Kapβ1 turnover and occupancy at the NPC in a RanGTP-dependent manner that is directly coupled to NLS-cargo release and NPC barrier function. This is underpinned by the binding affinity of Kapβ1 to phenylalanine–glycine nucleoporins (FG Nups), which is comparable with RanGTP·Kapβ1, but stronger for Kapα·Kapβ1. On this basis, RanGTP is ineffective at releasing standalone Kapβ1 from NPCs. Depleting Kapα·Kapβ1 by RanGTP further abrogates NPC barrier function, whereas adding back Kapβ1 rescues it while Kapβ1 turnover softens it. Therefore, the FG Nups are necessary but insufficient for NPC barrier function. We conclude that Kaps constitute integral constituents of the NPC whose barrier, transport, and cargo release functionalities establish a continuum under a mechanism of Kap-centric control.

Introduction

Nuclei physically segregate transcription from the cytoplasmic translation machinery in eukaryotic cells. Hence, gene expression relies on a controlled exchange of proteins and mRNA between the nucleus and cytoplasm. This is known as nucleocytoplasmic transport (NCT; Nigg, 1997; Görlich and Kutay, 1999; Stewart, 2007; Christie et al., 2016), which is regulated by three key elements: cargo-carrying karyopherin (Kap) receptors (specifically importins and exportins), the GTPase Ran, and aqueous channels that perforate the nuclear envelope (NE), known as nuclear pore complexes (NPCs; Eibauer et al., 2015; von Appen et al., 2015). Together, they facilitate the selectivity, transport efficiency, and accumulation of diverse cargoes in the nucleus.

NPCs are permeable to small molecules, but the entry of large, nonspecific entities is hindered (Popken et al., 2015; Timney et al., 2016). Tethered inside each NPC are several highly dynamic, intrinsically disordered proteins that impede the passage of nonspecific macromolecules (Sakiyama et al., 2016). These so-called phenylalanine–glycine nucleoporins (FG Nups) also harbor numerous FG repeats that bind Kaps (Rexach and Blobel, 1995; Bayliss et al., 2000; Allen et al., 2001), which achieve selective transport within milliseconds (Kubitscheck et al., 2005; Yang and Musser, 2006; Tu et al., 2013). Out of 20 members of the Kapβ family in humans, the 97-kD import receptor karyopherinβ1 (Kapβ1 or importin-β) regulates the canonical NCT pathway of diverse cargoes that comprise classical NLSs (NLS-cargo; Kimura et al., 2017). Kapβ1 itself does not bind classical NLS-cargoes directly but recruits a 58-kD adapter known as karyopherinα (Kapα or importin-α; Pumroy and Cingolani, 2015) that contains a C-terminal NLS-binding domain and an N-terminal autoinhibitory importin-β–binding (IBB) domain (Christie et al., 2016).

Current NPC models are FG centric and rely on the notion that the FG Nups reject nonspecific cargoes while promoting Kap-regulated transport. As a consequence, it remains a matter of debate whether the FG Nups resemble a gel-like permeability barrier (Frey and Görlich, 2007), a virtual gate (Rout et al., 2000) consisting of polymer brushes (Lim et al., 2007), or a mixture of gel and brush conformations (Yamada et al., 2010). In terms of their binding, individual FG repeats engage Kapβ1 by a rapid succession of multiple low-affinity interactions (Hough et al., 2015; Milles et al., 2015). Nevertheless, at equilibrium timescales, these manifest multivalent interactions that enhance binding affinity through avidity (Schoch et al., 2012; Kapinos et al., 2014). Approximately 1,000 selective translocation events ensue per NPC per second in both directions (Ribbeck et al., 1998), where 100 Kapβ1 molecules are estimated to occupy the pore at steady state (Paradise et al., 2007; Tokunaga et al., 2008; Lowe et al., 2015). We ourselves had shown that FG Nup layers undergo conformational changes

*L.E. Kapinos and B. Huang contributed equally to this paper.

Correspondence to Roderick Y.H. Lim: roderick.lim@unibas.ch

Abbreviations used: CD, circular dichroism; DOL, degree of labeling; IBB, importin-β binding; ITC, isothermal titration calorimetry; MST, microscale thermophoresis; NCT, nucleocytoplasmic transport; NE, nuclear envelope; Ni-NTA, nickel–nitrilotriacetic acid; NPC, nuclear pore complex; SPR, surface plasmon resonance.

The Rockefeller University Press
J. Cell Biol. Vol. 216 No. 11 3609–3624
https://doi.org/10.1083/jcb.201702092

to accommodate large numbers of Kapβ1 molecules depending on Kapβ1 concentration (Kapinos et al., 2014). At physiological Kapβ1 concentrations in particular, i.e., ∼10 µM (Paradise et al., 2007), we found that a pool of strongly bound Kapβ1 molecules occupies the FG Nups along with a more weakly bound pool that engages a reduced number of FG repeats. Indeed, evidence of these two pools can be found in the bimodal kinetics of exogenous Kapβ1 in digitonin-permeabilized cells (Lowe et al., 2015) and mRNA export in living cells (Grünwald and Singer, 2010). We therefore proposed a mechanism known as Kap-centric control whereby Kapβ1 occupancy in the FG Nups plays a role in regulating NPC barrier selectivity and transport speed (Lim et al., 2015).

Although NLS-cargo·Kapα·Kapβ1 complexes exhibit facilitated diffusion through the NPC (Yang et al., 2004), the release and accumulation of NLS-cargo in the nucleus is energetically activated. This is regulated by the small GTPase Ran, which has GTP- and GDP-bound forms that are asymmetrically distributed in the nucleus and cytoplasm, respectively (Görlich et al., 1996; Weis et al., 1996; Lyman et al., 2002). Importantly, RanGTP functionally releases both NLS-cargo and Kapα in the nucleus upon binding Kapβ1 (Görlich et al., 1996; Catimel et al., 2001; Stewart, 2007), after which RanGTP·Kapβ1 complexes are exported back to the cytoplasm (i.e., turned over) for eventual reuse.

Whereas the aforementioned processes define individual aspects of NCT, the manner by which NPC barrier selectivity, Kap exchange, and NLS-cargo release function simultaneously under equilibrium conditions remains incoherent. As a matter of fact, each of these processes involves Kapβ1, which binds Kapα in the cytosol to ferry NLS-cargoes, FG Nups to bypass the NPC, and RanGTP in the nucleus to deliver cargo. Hence, the binding of one partner may well impact on another to influence the entire transport continuum. One peculiarity pertains to Kapβ1 turnover, where a prevailing notion claims that RanGTP concomitantly promotes Kapβ1 dissociation from the FG Nups after cargo delivery into the nucleus (Rexach and Blobel, 1995). This is based on in vitro evidence showing that RanGTP abolishes Kapβ1–FG Nup interactions (or more exactly, Kap60 from Kap95 in some cases; Rexach and Blobel, 1995; Floer et al., 1997; Ben-Efraim and Gerace, 2001; Lyman et al., 2002; Lim et al., 2007). When lacking FG Nup binding, however, the as-formed RanGTP·Kapβ1 complex would itself resemble a nonspecific cargo whose export via NPCs (i.e., Kapβ1 turnover) violates NCT selectivity. To add to the confusion, recombinant Kapβ1 is typically retained at the NE of permeabilized cells, whereas Kapα and NLS-cargoes accumulate within the nucleoplasm when RanGTP is present (Görlich et al., 1995; Moroianu et al., 1995).

In this work, we have combined biophysical quantitation and functional permeabilized cell assays to explore the molecular interconnections between NPC barrier function, Kapβ1 occupancy, turnover, and NLS-cargo release. First, we used surface plasmon resonance (SPR) to measure the effect of RanGTP on the binding affinities of Kapβ1, Kapα·Kapβ1, and MG-NLS·Kapα·Kapβ1 (where MG-NLS is a 76-kD maltose-binding protein (MBP)–GFP-NLS cargo fusion protein) to the FG Nups along with associated conformational changes in FG Nup layers. Second, we analyzed the concentration dependence and stoichiometry of different Kapβ1 complexes and their combined influence on FG Nup binding. Third, we validated the respective in situ behaviors using digitonin-permeabilized cells. Our results show that Kapα·Kapβ1 exhibits a pronounced binding and occupancy at the NPCs. RanGTP triggers the release of both Kapα and NLS-cargo by converting Kapα·Kapβ1 to RanGTP·Kapβ1, which binds the FG Nups more weakly and leads to reduction in total Kapβ1 occupancy. However, RanGTP has no eluting effect on standalone Kapβ1 because RanGTP·Kapβ1 shares the same binding affinity to the FG Nups as Kapβ1. Finally, depleting Kapα·Kapβ1 by RanGTP abrogates NPC barrier function, which is rescued by adding back either Kapβ1 or Kapα·Kapβ1. Still, under active transport conditions, Kapβ1 turnover leads to a softening of the barrier. It therefore follows that Kapα mediates Kapβ1 occupancy and turnover in a RanGTP-dependent manner to impart Kap-centric control at the NPC.

Results

Binding of RanGTP·Kapβ1 to FG Nups

SPR was used to correlate in situ equilibrium and kinetic aspects of RanGTP·Kapβ1 binding to conformational changes in Nup214, Nup62, Nup98, and Nup153 (denoted as cNup214, cNup62, cNup98, and cNup153). As before, this uses BSA to probe FG layer height (Fig. S1; Schoch et al., 2012; Kapinos et al., 2014). Before SPR experimentation, all Kaps and transport complexes were characterized in aqueous solution using isothermal titration calorimetry (ITC), microscale thermophoresis (MST), and circular dichroism (CD; Fig. S2). This gave an equilibrium dissociation constant of K_d = 35 ± 12.5 nM for RanGTP·Kapβ1, which compares well with previous estimates (Bednenko et al., 2003; Hahn and Schlenstedt, 2011; Lolodi et al., 2016). Thereafter, we applied RanGTP·Kapβ1 (1.5:1) ranging from 10 nM to 20 µM Kapβ1, giving RanGTP·Kapβ1 fractions of 25% up to 100% for the SPR experiments (Fig. 1 A). Thus, the FG Nups typically interacted with RanGTP·Kapβ1 in a diminishing background of free Kapβ1 (and RanGTP) with increasing Kapβ1 concentration. Upon completion of a binding sequence (Fig. 1 B), each FG Nup layer was regenerated by NaOH treatment to remove RanGTP·Kapβ1. We then measured how RanGTP binds to standalone Kapβ1–FG Nup complexes to compare the two scenarios.

RanGTP·Kapβ1–FG Nup binding is accompanied by an incremental increase in the FG Nup layer height that plateaus at the highest RanGTP·Kapβ1 concentrations (Fig. 1 C). This behavior, which differs quantitatively between FG Nups, likely originates from differences in their intrinsic properties. However, there are qualitative similarities to the binding of standalone Kapβ1 (Kapinos et al., 2014) that signifies FG Nup saturation at micromolar RanGTP·Kapβ1 concentrations. Nevertheless, there is a slight height increase for RanGTP·Kapβ1 over standalone Kapβ1 because of the larger hydrodynamic diameter of RanGTP·Kapβ1 (9.6 ± 1.3 nm) compared with standalone Kapβ1 (6.8 ± 1.8 nm; Table S1). Moreover, RanGTP binding to preformed Kapβ1–FG Nup layers elicits further increases in height, as opposed to a decrease as one would expect if RanGTP·Kapβ1 would subsequently unbind. Hence, it is evident that RanGTP does not facilitate the release of standalone Kapβ1 from the FG Nups.

Influence of RanGTP on Kapα·Kapβ1–FG Nup binding

Next, we sought to determine how Kapα·Kapβ1 complexes interact with the FG Nups and how RanGTP might affect their

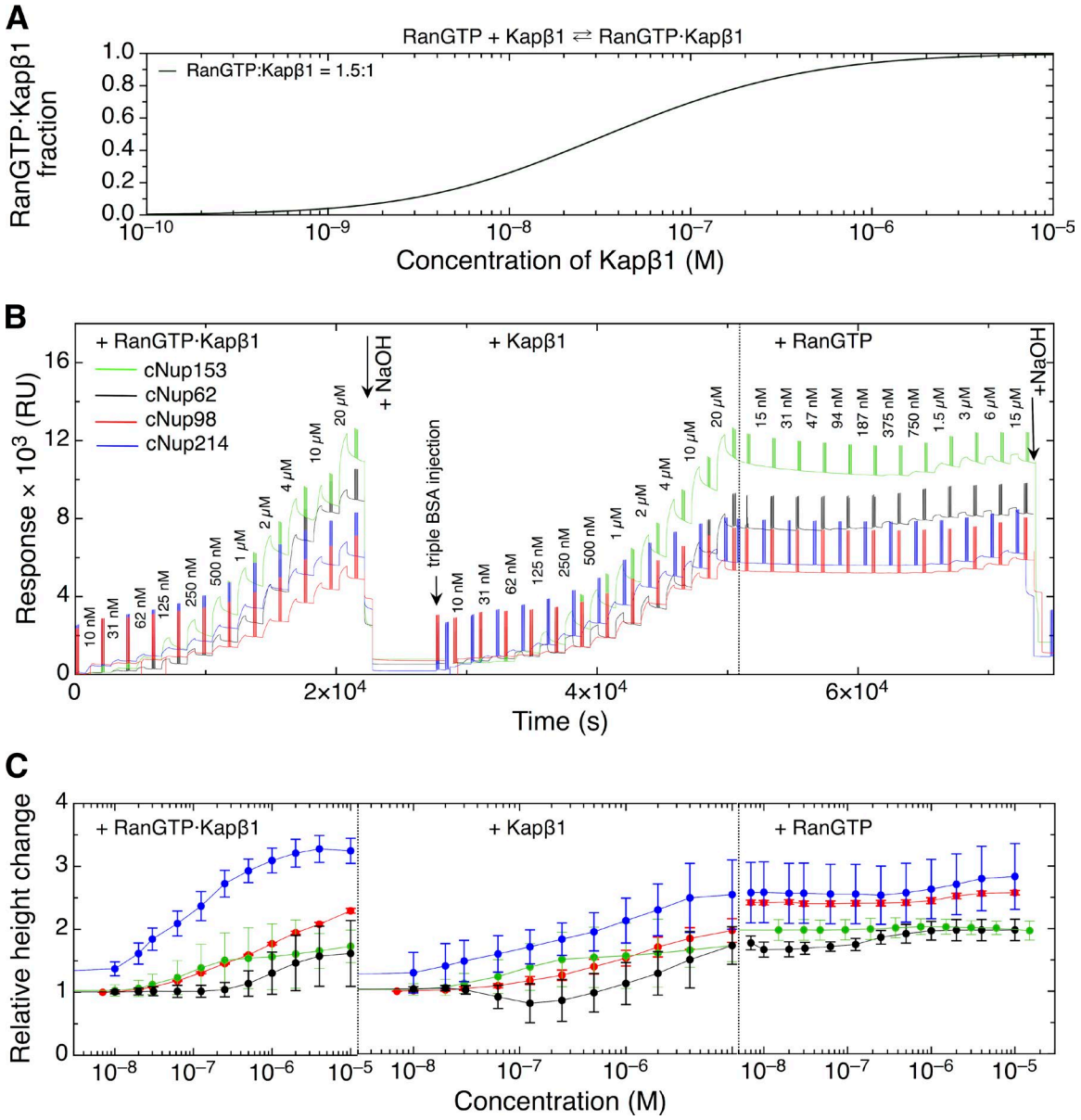

Figure 1. **RanGTP does not dissociate standalone Kapβ1 from the FG Nups.** (A) Calculated solution binding isotherm for RanGTP/Kapβ1 at a ratio of 1.5:1 with K_d = 35 nM. (B) SPR response curves for RanGTP·Kapβ1 binding to different FG Nups followed by injections of Kapβ1 and RanGTP after a NaOH regeneration step. Vertical signals correspond to triple BSA injections that are used to measure FG Nup layer height. RU, resonance units. (C) Corresponding height changes to the FG Nup layer with respect to B. n = 10 per FG Nup. Error bars denote standard deviation.

binding. As before, ITC determination gave an equilibrium dissociation constant of K_d = 210 ± 77 nM for Kapα-Kapβ1 binding (Fig. S2 B), in good agreement with previous values (Falces et al., 2010). At a mixing ratio of 1.5:1, ∼40% Kapα·Kapβ1 was expected to form at 100 nM Kapβ1, and this reaches ∼80% at 1 µM and 95% at 10 µM Kapβ1 (Fig. 2 A). Therefore, in our SPR assay, Kapα·Kapβ1 complexes interacted with the FG Nups in a background of free Kapα and Kapβ1, which diminished as Kapα·Kapβ1 concentration increased.

After reaching 20 µM Kapα·Kapβ1, up to 15 µM RanGTP was added to test its efficacy to dissociate Kapα. In marked contrast to Fig. 1 C, RanGTP led to reductions in both the Kapα·Kapβ1–FG Nup binding response and layer height (Fig. 2, B and C), except for cNup98, potentially because of its lower capacity to bind Kapβ1 than the other FG Nups (Kapinos et al., 2014). We attribute this decrease to the release of Kapα after the conversion of Kapα·Kapβ1 to RanGTP·Kapβ1. This is reasonable given that the exchange of Kapα (58 kD) to RanGTP (26 kD) leads to a reduction in total FG Nup–bound mass (Fig. 2 C). Likewise, we observed similar behavior when MG-NLS·Kapα·Kapβ1 was bound to cNup153, indicating that RanGTP-Kapβ1 binding triggered the release of MG-NLS and Kapα from the FG Nup layer (Fig. S3).

Separately, we found that RanGTP·Kapβ1 exhibited promiscuous binding interactions (Wagner et al., 2015) with preformed Kapα·Kapβ1–FG Nup layers, which led to an increase in both the SPR signal and layer height (Fig. S3, D and E). Hence, this indicates that RanGTP·Kapβ1 and Kapα·Kapβ1 can simultaneously bind and coexist within the FG Nups without directly interacting with one another.

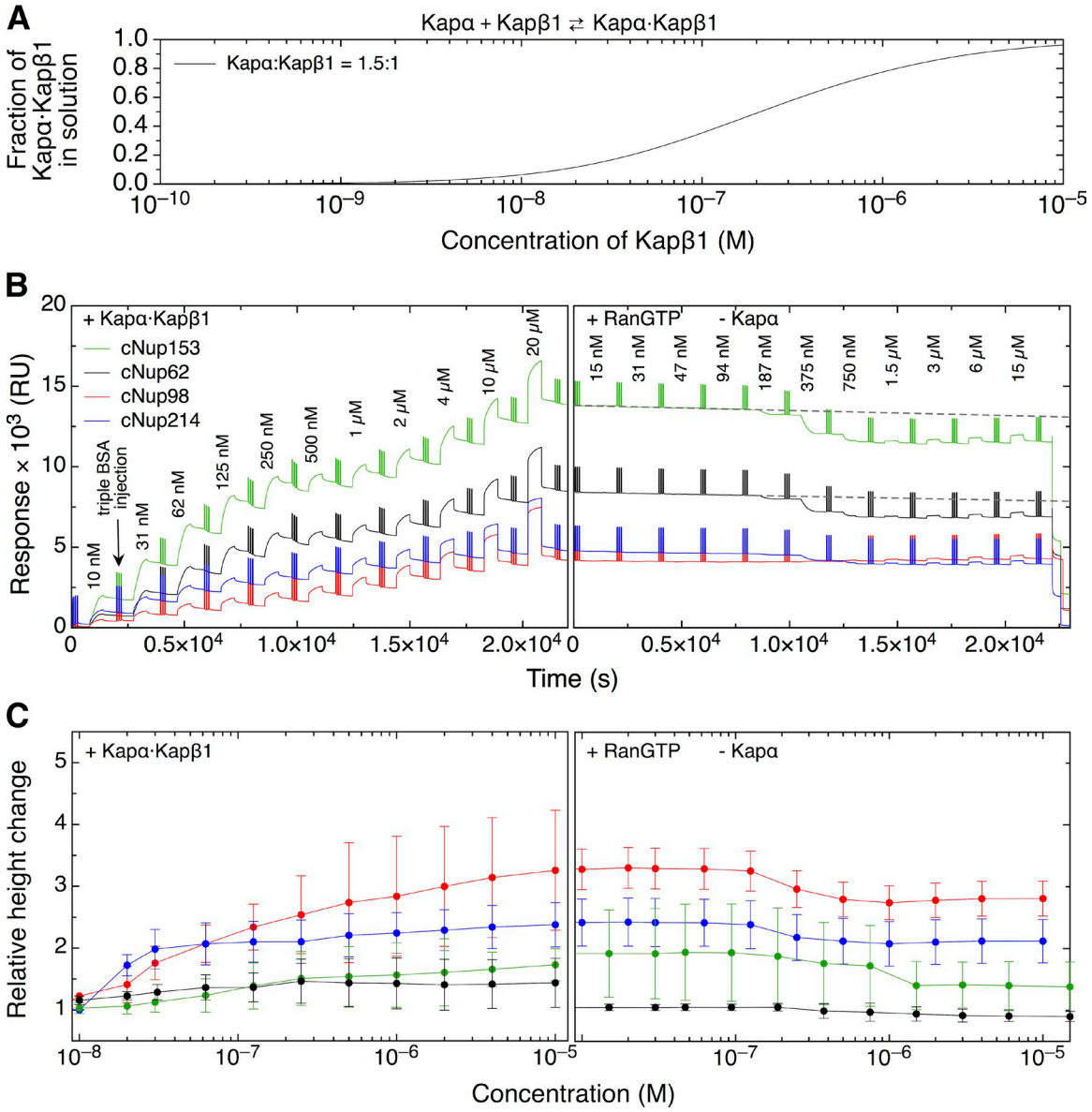

Figure 2. **RanGTP dissociates Kapα from FG Nup–bound Kapα·Kapβ1.** (A) Solution binding isotherm calculated for Kapα/Kapβ1 at a ratio of 1.5:1 with K_d = 210 nM. (B) SPR response curves for Kapα·Kapβ1 binding to different FG Nups show that Kapα is eluted by RanGTP. Vertical signals correspond to triple BSA injections that are used to measure FG Nup layer height. RU, resonance units. (C) Corresponding height changes to the FG Nup layer with respect to B. n = 10 per FG Nup. Error bars denote standard deviation.

Comparing Kapβ1, Kapα·Kapβ1, MG-NLS·Kapα·Kapβ1, and RanGTP·Kapβ1 binding to FG Nups

Fig. 3 A summarizes the affinities associated with the binding of each transport complex to the FG Nups as determined from Langmuir isotherm analysis (Fig. S4 A). Indeed, all four entities exhibit two-phase binding interactions with the FG Nups with distinct affinities at the ∼0.1 µM (strong) and ∼10 µM (weak) ranges. These two binding regimes are also distinguishable by their kinetic behavior (Fig. S4 B), where (a) strong binding (lower K_d) is associated with fast on-rates (k_{on}) and slow off-rates (k_{off}), thereby suggesting that uptake into unsaturated FG Nup layers is rapid and stable; and (b) weak binding (higher K_d) of near-saturated FG Nup layers comes from a reduction in k_{on} and increase in k_{off} being a characteristic of more transient interactions.

Interestingly, Kapα·Kapβ1 has a 10-fold higher affinity (lower K_d) in the strong binding phase than Kapβ1 and RanGTP·Kapβ1, which are overall similar. This indicates that Kapα·Kapβ1 complexes are more stable when binding FG Nups than Kapβ1 or RanGTP·Kapβ1. However, this is unexpected because Kapα itself does not bind the FG Nups (Fig. S4 C) with the exception of cNup153, which binds Kapα weakly, i.e., K_d = 1.3 ± 0.1 µM because of an NLS-like sequence at its C terminus (Makise et al., 2012; Ogawa et al., 2012). Nevertheless, Kapα·Kapβ1 complexes seem to be less flexible than free Kapβ1 molecules, and this might serve to stabilize the binding of Kapα·Kapβ1 to the FG Nups (Cingolani et al., 2000; Tauchert et al., 2016). Still, MG-NLS·Kapα·Kapβ1–FG Nup binding is not measurably stronger than Kapα·Kapβ1 (Fig. 3 and Fig. S4 D), which suggests that MG-NLS does not influence their binding.

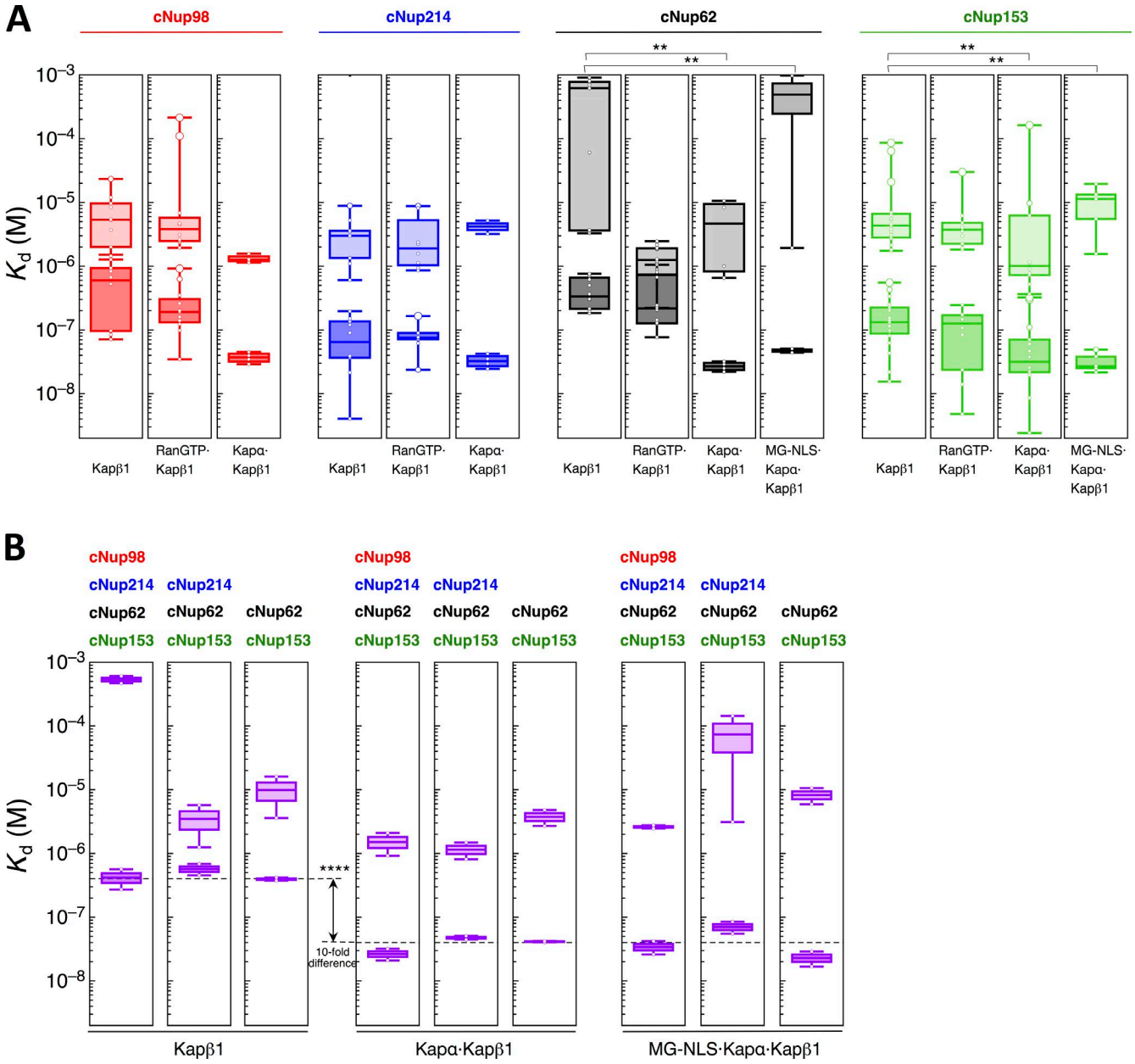

Figure 3. **FG Nups bind Kapα·Kapβ1 more strongly than Kapβ1 and RanGTP·Kapβ1, which are similar.** (A) FG Nup binding of Kapβ1 and related transport complexes are characterized by two distinct equilibrium dissociation constants at ∼0.1 µM (strong) and ∼10 µM (weak). In all cases, Kapα switches the Kapβ1 complex to a quantitatively higher binding affinity (lower K_d). RanGTP lowers the binding state to a value that is comparable with standalone Kapβ1. MG-NLS cargo does not significantly affect Kapα·Kapβ1 binding to Nup153 and Nup62. **, P < 0.01; Student's *t* test (see Table S3). (B) Kapα·Kapβ1 and MG-NLS·Kapα·Kapβ1 have a quantitatively higher binding affinity (lower K_d) than Kapβ1 when binding mixed FG Nups. To aid comparison, dashed lines at K_d values of 40 and 400 nM show that Kapα·Kapβ1 or MG-NLS·Kapα·Kapβ1 binds the FG Nups 10-fold stronger than standalone Kapβ1. ****, P < 0.0001; Student's *t* test. Box plots denote the median, first, and third quartiles. Error bars denote standard deviation, including outliers.

To more closely mimic binding in the NPC, we also tested mixed layers comprised of different FG Nup combinations. As before, we observed a similar ∼10-fold higher affinity of Kapα·Kapβ1 and MG-NLS·Kapα·Kapβ1 over standalone Kapβ1, regardless of the FG Nup layer composition (Fig. 3 B). Based on these results, we hypothesized that Kapα release is essential for Kapβ1 turnover because Kapβ1–FG Nup affinity is most effectively reduced when RanGTP replaces Kapα to bind Kapβ1 (i.e., RanGTP·Kapβ1 > K_d > Kapα·Kapβ1). Importantly, this provides further evidence that RanGTP does not facilitate the release of standalone Kapβ1 from the FG Nups (i.e., RanGTP·Kapβ1 ≈ K_d ≈ Kapβ1).

Equilibrium analysis of RanGTP·Kapβ1 dissociation from the FG Nups

RanGTP concomitantly liberates Kapα and NLS-cargoes upon binding Kapβ1. However, it remains unclear to what extent RanGTP·Kapβ1 dissociates from the FG Nup layer. A technical limitation of SPR is that the relative amount of different Kapβ1 complexes that bind the FG Nups is not obvious. To be precise, the overall binding response at equilibrium (R_{eq}) is proportional to the amounts of standalone Kapβ1, Kapα·Kapβ1, and MG-NLS·Kapα·Kapβ1 complexes that coexist in solution and their respective affinities to the FG Nups (Fig. S5 A). This is further determined by their respective binding iso-

therms that vary as a function of their molar concentrations and ratio (Sun et al., 2013).

Three parallel reactions then proceed in the presence of RanGTP (Fig. S5, B–D). First, RanGTP binds standalone Kapβ1, which has a minimal impact on Kapβ1–FG Nup binding. Second, RanGTP converts Kapα·Kapβ1 to RanGTP·Kapβ1, which facilitates Kapβ1 dissociation and concomitantly elutes Kapα. Third, RanGTP elutes Kapα and MG-NLS cargo by converting MG-NLS·Kapα·Kapβ1 to RanGTP·Kapβ1, which likewise promotes Kapβ1 dissociation from the FG Nups. To correlate these behaviors, we tested the effect of 5 µM RanGTP on increasing ratios of MG-NLS/Kapα/Kapβ1 (ranging from 1:1:4 to 10:10:1) against cNup153 (Fig. S5 E). Moreover, this was repeated at three specific Kapβ1 concentrations ($C_{Kapβ1}$): 10, 100, and 1,000 nM (Fig. S5, E–G). We note that the change in the normalized equilibrium binding response (ΔR_{norm}) at each Kapβ1 concentration would then depend solely on the ratio between different Kapβ1 complexes because the absolute number of Kapβ1 molecules remains the same.

Overall, RanGTP elicited the largest reduction of total FG Nup–bound mass at 100 nM Kapβ1, which diminishes below ∼10 nM and above 1 µM Kapβ1. This nonmonotonic behavior agrees qualitatively with equilibrium calculations (Fig. 4 and Fig. S5 G), which explain that (a) the number of Kapβ1–FG binding complexes is small at 10 nM Kapβ1; (b) total Kapβ1 reduction at the FG Nups is greatest at 100 nM, being close to the affinity (K_d) of RanGTP·Kapβ1, Kapα·Kapβ1, and MG-NLS·Kapα·Kapβ1; and (c) reduction is diminished at 1 µM Kapβ1 because of a saturation of Kapβ1 complexes. Moreover, the reduction in binding response (ΔR_{norm}) scales with the amount of eluted Kapα and MG-NLS as well as RanGTP·Kapβ1 dissociation (ΔKapβ1) as defined by MG-NLS/Kapα/Kapβ1 ratios. Hence, Kapβ1 dissociation from the FG Nups is directly coupled to Kapα/NLS-cargo release by the action of RanGTP.

RanGTP facilitates Kapβ1 turnover at NPCs by eluting Kapα

With the biophysical insights noted above, we sought to confirm whether Kapα did indeed play a role in facilitating the release of Kapβ1 from functional NPCs in a series of digitonin-permeabilized cell assays (Fig. 5 A). We had previously shown that a pool of endogenous Kapβ1 (endoKapβ1) persisted at the NE for a prolonged duration after permeabilization (Lim et al., 2015). Upon confirming that endogenous Kapα (endoKapα) colocalizes with endoKapβ1 at the NE, we used Ran mix, which reinstates the soluble transport machinery to power NCT in permeabilized cells (Görlich et al., 1995). This consisted of 5 µM RanGDP, 4 µM NTF2, and an energy-regenerating system (2 mM GTP, 0.1 mM ATP, 4 mM creatine phosphate, and 20 U/ml creatine kinase) in transport buffer. After Ran mix treatment, immunofluorescence assays showed that endoKapβ1 was significantly depleted at the NE (Fig. 5 B). Importantly, this ensured that the NPCs were as close as possible to a ground state, i.e., vacant, to minimize interference with the binding and retention of its exogenous counterparts. We then incubated the permeabilized cells in exogenous Kapβ1 (i.e., Kapβ1–Alexa Fluor 568; hereafter denoted as exoKapβ1) followed by a second Ran mix treatment to evaluate exoKapβ1 turnover. Interestingly, standalone exoKapβ1 was poorly displaced from the NPCs (Fig. 5 C), thereby corroborating our biophysical analyses showing that RanGTP does not facilitate the turnover of standalone Kapβ1 (Fig. 1).

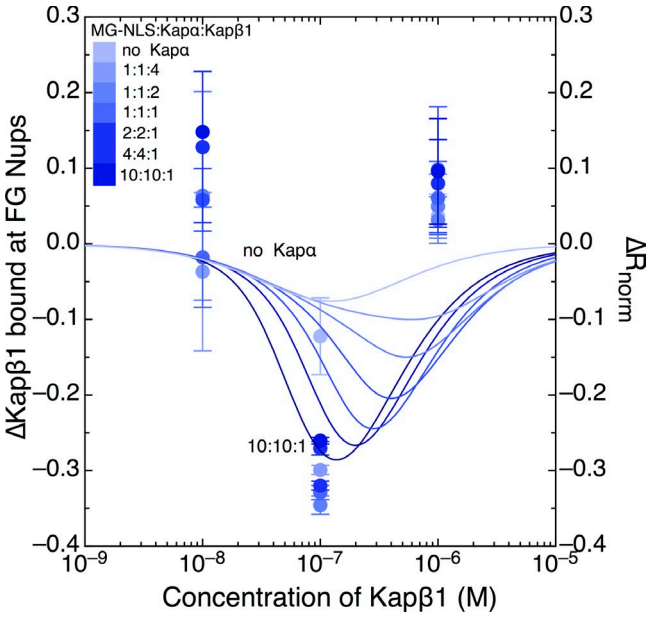

Figure 4. **FG Nup binding efficiency depends on MG-NLS/Kapα/Kapβ1 ratio, concentration, and RanGTP.** Relative decrease of FG Nup–bound Kapβ1 due to RanGTP at different MG-NLS/Kapα/Kapβ1 ratios. A maximal reduction of Kapβ1 occurs when MG-NLS/Kapα/Kapβ1 = 10:10:1. Varying MG-NLS/Kapα/Kapβ1 ratios at constant $C_{Kapβ1}$ = 10, 100, and 1,000 nM enables comparisons between experiment (ΔR_{norm}; colored dots) and equilibrium calculations (ΔKapβ1; colored lines). For more information, see Fig. S5.

Thereafter, we wanted to verify that exoKapα was required for facilitating exoKapβ1 turnover at NPCs using RanGTP. We then incubated endoKap-depleted permeabilized cells in 10:1 ratios of exoKapα (i.e., Kapα–Alexa Fluor 488) and exoKapβ1 for $C_{Kapβ1}$ = 10 nM and 100 nM and a 4:1 ratio for $C_{Kapβ1}$ = 1 µM, with a calculated coupling efficiency of 30, 80, and 95%, respectively, to remain consistent with our biophysical analyses. Before Ran mix treatment, exoKapβ1 was distinctly localized to the NE, whereas exoKapα was located both at the NE and within the nucleus as observed previously (Fig. 5 D; Görlich et al., 1995). This can be attributed to the slow natural dissociation of exoKapα from exoKapβ1 in the absence of RanGTP (Catimel et al., 2001). After Ran mix treatment, however, both exoKapα and exoKapβ1 reduced in a nonmonotonic manner (as predicted by our equilibrium calculations) with a maximum reduction of ∼50% at $C_{Kapβ1}$ = 100 nM (Fig. 5, E and F). This therefore confirms that Kapα facilitates Kapβ1 turnover in a RanGTP-dependent manner.

Kapβ1 depletion abrogates NPC barrier function

Next, we asked whether the retained pool of endoKapα·endo Kapβ1 might play a role in reinforcing the FG Nup barrier, as we had hypothesized previously (Lim et al., 2015). Separately, we applied 1 µM MG (MBP-GFP) nonspecific cargoes that lacked the NLS and 1 µM MG-NLS specific cargoes to test for nuclear leak-in (Fig. 6 A). Indeed, both cargoes did not permeate into the nucleus when endoKapα·endoKapβ1 was present (Fig. 6 B). Surprisingly, however, both cargoes readily entered into the nucleus upon depleting the NE of endoKapα·endoKapβ1 by Ran mix (Fig. 6 C). Moreover, adding back only 100 nM exoKapβ1 sufficiently restored

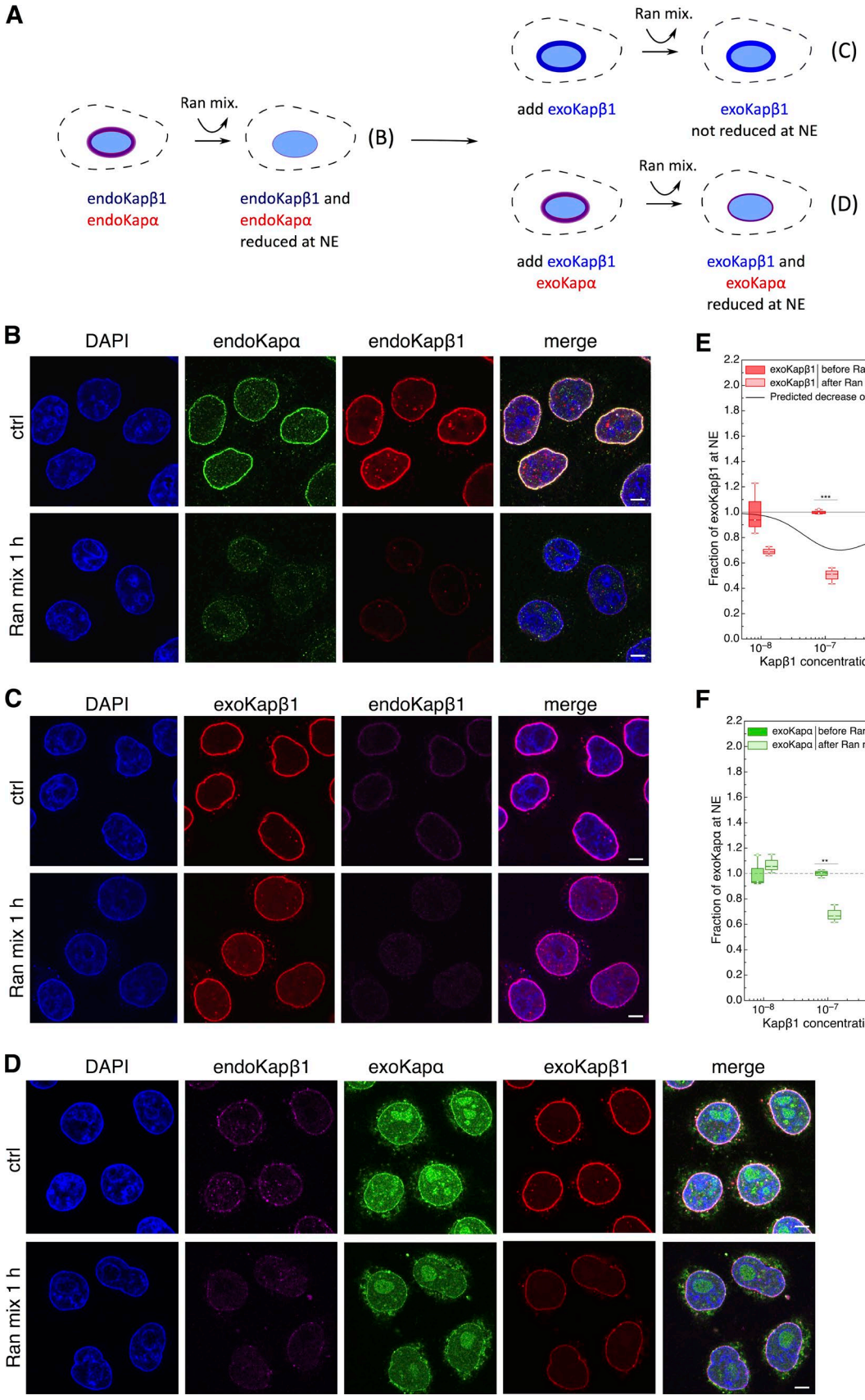

Figure 5. **Kapα facilitates the RanGTP-mediated release of Kapβ1.** (A) Cartoon illustration of the experiment. (B) Immunofluorescence reveals that endoKapα and endoKapβ1 are retained and colocalize at the NE after permeabilization. Ran mix treatment effectively leads to a reduction in both endogenous pools. (C) ExoKapβ1 is not reduced by Ran mix after repopulating endoKap-reduced NPCs with 100 nM exoKapβ1. (D) Ran mix effectively reduces

the NPC barrier to prevent the passive transport of both cargoes into the nucleus (Fig. 6, D–F). Hence, this proves that Kapβ1 occupancy regulates NPC barrier function by reinforcing the FG Nups against the passive transport of macromolecular cargoes.

Kapβ1 turnover at NPCs is coupled to NLS-cargo release

Then, we sought to correlate the active transport of MG-NLS into the nucleus with the RanGTP-dependent reduction of exo Kapβ1 and release of exoKapα from NPCs (Fig. 7 A). A key objective was to elicit comparisons between permeabilized cell assays and the equilibrium analyses (Fig. 4 and Fig. S5). As mentioned above, we incubated endoKap-depleted permeabilized cells with 10:1 ratios of exoKapα and exoKapβ1 for $C_{Kapβ1}$ = 10 nM and 100 nM and a 2:1 ratio for $C_{Kapβ1}$ = 1 µM, supplemented with 1 µM MG-NLS. The MG-NLS concentration was fixed to facilitate direct comparisons with respect to their nuclear uptake between experiments. Consequently, Ran mix affected exoKapβ1 in the same nonmonotonic manner as when MG-NLS was absent (Fig. 5 E), leading to a maximum reduction of 41% at 100 nM exoKapβ1 (Fig. 7, B and C). Even so, Ran mix treatment did not completely dissociate exoKapα from the NE (Fig. 7 D). This may be explained by complex formation with its export receptor, cellular apoptosis susceptibility protein (CAS) and RanGTP (Kutay et al., 1997a) at the NPC.

In parallel, the passive transport of MG-NLS into the nucleus increased with exoKapα/exoKapβ1 concentration before Ran mix treatment, which is consistent with the findings of Yang and Musser (2006). After this, Ran mix facilitated an active nuclear uptake of MG-NLS (Fig. 7 E). However, this had a rather low significant difference, likely because of dilution inside the nucleus. In any case, MG-NLS signal increase is more apparent at 100 nM exoKapβ1, but less so at 1 µM exoKapβ1, because of the use of a 2:1 ratio of exoKapα/exoKapβ1 in the latter experiment. Still, neither exoKapβ1 reduction nor an active uptake of MG-NLS proceeded in control experiments that excluded exo Kapα (Fig. 7, F and G). Hence, Kapβ1 turnover at NPCs is facilitated by Kapα and is directly coupled to NLS-cargo release.

Kapβ1 turnover softens the NPC barrier

Finally, we wanted to ascertain the fate of nonspecific cargoes under the same exogenous conditions. As before with only exo Kapβ1 at the NE (Fig. 6 D), passive nuclear entry of MG was forbidden in permeabilized cells pretreated with exoKapα·exo Kapβ1. However, in the presence of Ran mix, we observed a marginal uptake of MG correlated to exoKapβ1 reduction at the NE (Fig. 8), though not to the same extent as when the NPCs were vacant (Fig. 6 C). This indicates that the NPC barrier is less rigid under active transport conditions, which is consistent with in vivo observations of nonspecific transport (Popken et al., 2015; Timney et al., 2016).

Discussion

Kapα facilitates Kapβ1 turnover to regulate NPC function

Kapα plays a key role in unifying selective barrier, transport, and cargo release functionalities at the NPC to regulate NCT. We anticipate that mainly NLS-cargo·Kapα·Kapβ1 complexes populate the NPCs in vivo rather than their standalone equivalents. Beyond its role as an adapter for NLS-cargo, Kapα appears functionally important for switching on the high-affinity state of Kapβ1 toward the FG Nups to promote NLS-cargo import. RanGTP then downgrades this complex to a state of lower affinity to facilitate the turnover of RanGTP·Kapβ1 from the NPC. Interestingly, the softening of the NPC barrier (Fig. 8, B and C; Popken et al., 2015; Timney et al., 2016) that follows might place an upper limit on space constraints within the pore to maintain transport speed and accessibility. Still, because of their lack of cross-reactivity, both NLS-cargo·Kapα·Kapβ1 and RanGTP·Kapβ1 can co-exist in a dynamic equilibrium at the NPC to maintain nucleocytoplasmic transport.

Kapβ1–FG Nup binding affinity depends on Kapα and RanGTP

At the molecular level, MG-NLS·Kapα·Kapβ1, Kapα·Kapβ1, RanGTP·Kapβ1, and standalone Kapβ1 can all bind FG Nups, though MG-NLS·Kapα·Kapβ1 and Kapα·Kapβ1 exhibit a higher affinity for the FG Nups than RanGTP·Kapβ1 and standalone Kapβ1, which are similar (Fig. 3). This is consistent with the increased binding of IBB·Kap95 to the FG Nups over standalone Kap95 and RanGTP·Kap95 (Eisele et al., 2010). However, it disagrees with the notion that RanGTP either completely (Delphin et al., 1997; Floer et al., 1997; Ben-Efraim and Gerace, 2001) or partially (Allen et al., 2001; Pyhtila and Rexach, 2003) diminishes FG repeat interactions with standalone Kapβ1 to facilitate its release from NPCs. Previously, we had reported that Kapβ1 binding induced a conformational compaction in cNup153 that was reversible with excess RanGTP (Lim et al., 2007). Given our present insights, RanGTP likely facilitated Kapβ1 release as a result of the extremely low binding efficiency of Kapβ1 to cNup153 at the sub-nanomolar concentrations used.

Structural evidence for the enhanced binding of Kapα·Kapβ1

From a structural perspective, Kapβ1 is a flexible α-helical solenoid consisting of 19 tandem HEAT repeats (Cingolani et al., 1999, 2000; Bayliss et al., 2000; Fukuhara et al., 2004; Lee et al., 2005; Zachariae and Grubmüller, 2008; Yoshimura et al., 2014). Not surprisingly, the Kapβ1 structure is sensitive to solvent conditions (Forwood et al., 2008, 2010; Halder et al., 2015) and Kapα/IBB (Cingolani et al., 1999, 2000; Lee et al., 2005). Because of their overlapping binding sites on Kapβ1, RanGTP is known to trigger structural rearrangements within Kapβ1 to release Kapα/IBB (Conti et al., 2006), but how it modulates the affinity of Kapβ1 toward the FG Nups

exoKapβ1 after repopulating endoKap-reduced NPCs with exoKapα·exoKapβ1 (Kapα/Kapβ1 = 10:1; $C_{Kapβ1}$ = 100 nM). (E) From D, exoKapβ1 retention at the NE after Ran mix (light red) shows qualitative agreement with equilibrium calculations (solid line) as a function of exoKapβ1 concentration. To aid comparison, these values were normalized by preRan mix values (dark red). (F) From D, exoKapα retention at NE before (dark green) and after Ran mix (light green). **, P < 0.01; ***, P < 0.001. Student's *t* test (see Table S3). Box plots denote the median, first, and third quartiles. Error bars denote standard deviation, including outliers. Bars, 5 µm. In C and D, an endogenous protein-specific antibody that does not cross react with exoKapβ1 was used to immunostain for endoKapβ1. See Materials and methods for details.

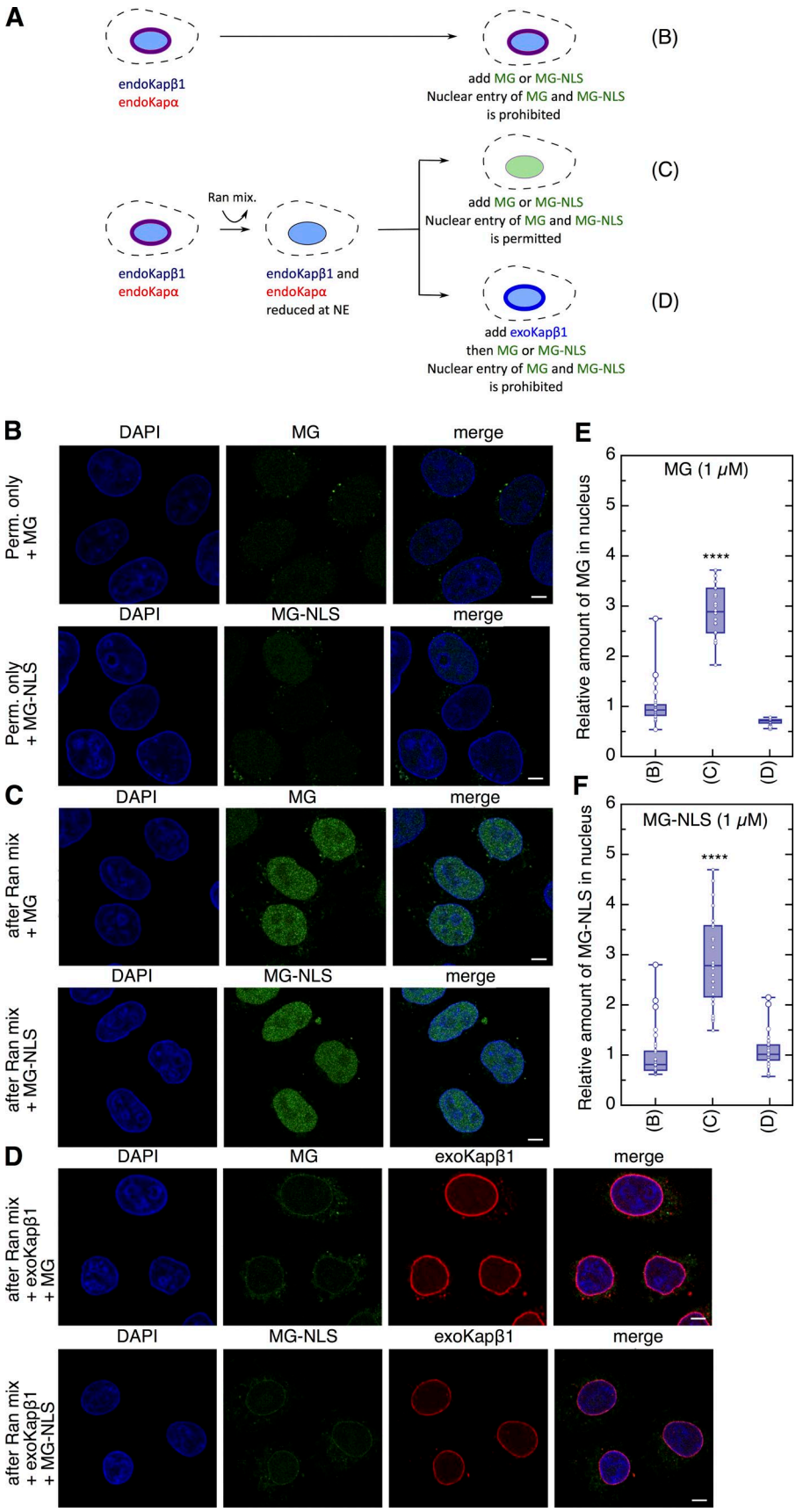

Figure 6. **FG Nups are necessary but insufficient for NPC barrier function.** (A) Cartoon illustration of all experiments. (B) Nuclear entry of MG and MG-NLS is prohibited in the presence of endoKapα and endoKapβ1 immediately after digitonin permeabilization. (C) Depleting endoKapα and endoKapβ1 by Ran mix abrogates NPC barrier function and facilitates the passive entry of MG and MG-NLS into the nucleus. (D) Adding back 100 nM exoKapβ1 sufficiently rescues NPC barrier function to prohibit MG and MG-NLS from entering the nucleus. (E) Fluorescence quantitation of MG in the nucleus at each of the above conditions. (F) Fluorescence quantitation of MG-NLS in the nucleus at each of the above conditions. n = 3 per experimental condition with a total of at least 26 cells each. ****, $P < 0.0001$; Student's t test. Box plots denote the median, first, and third quartiles. Error bars denote standard deviation, including outliers. Bars, 5 µm.

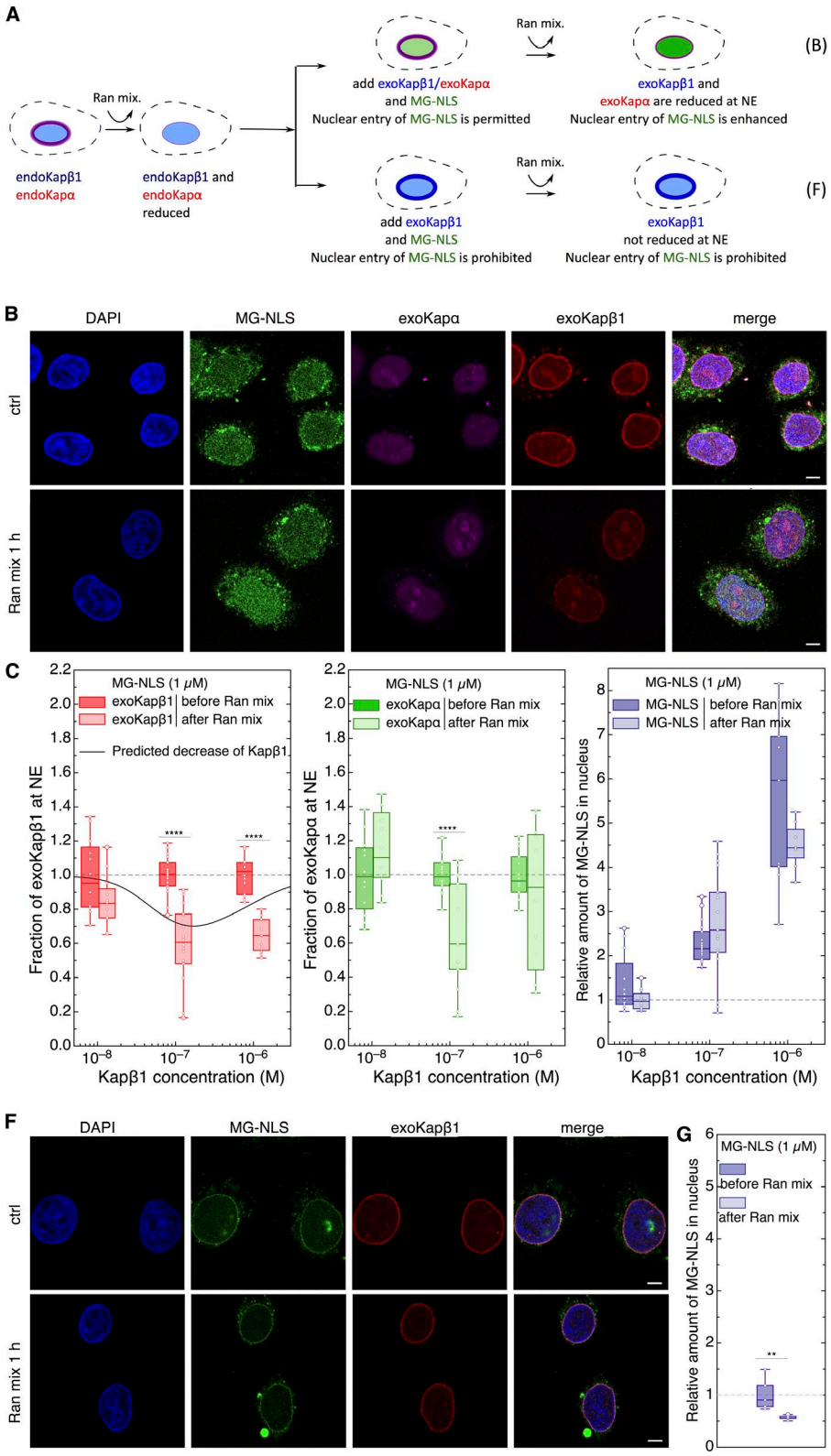

Figure 7. **Kapβ1 turnover at NPCs is directly coupled to NLS-cargo release.** (A) Cartoon illustration of all experiments. (B) Ran mix effectively reduces exoKapβ1 after repopulating endoKap-reduced NPCs with MG-NLS·exo Kapα·exoKapβ1. (C) ExoKapβ1 retention at the NE after Ran mix (light red) shows qualitative agreement with equilibrium calculations (solid line) as a function of exoKapβ1 concentration. To aid comparison, these values were normalized by preRan mix values (dark red). (D) ExoKapα retention at NE before (dark green) and after Ran mix (light green). (E) Comparison of passive (dark purple) and Ran mix–activated (light purple) accumulation of MG-NLS in the nucleus. (F) Neither passive nor Ran mix–activated nuclear entry of MG-NLS was permitted in NPCs repopulated with exoKapβ1 (no exoKapα). ExoKapβ1 does not turn over under these conditions. (G) Fluorescence quantitation of nuclear MG-NLS before (dark purple) and after Ran mix (light purple) from F. $n = 3$ per experimental condition with a total of 10–12 cells each. **, $P < 0.01$; ****, $P < 0.0001$; Student's t test. Box plots denote the median, first, and third quartiles. Error bars denote standard deviation, including outliers. Bars, 5 µm.

remains unclear. Previous studies show that Kapα·Kapβ1 is more structurally compact than RanGTP·Kapβ1 (Cingolani et al., 1999; Fukuhara et al., 2004; Lee et al., 2005), and this might stabilize FG repeat binding on the outer Kapβ1 surface (Bayliss et al., 2000; Bednenko et al., 2003; Isgro and Schulten, 2005). It may be that the flexibility of RanGTP·Kapβ1 or standalone Kapβ1 incurs a higher entropic penalty for FG repeat binding. In any case, there is no obvious structural evidence that argues against the accessibility of FG repeats to bind RanGTP·Kapβ1. Furthermore, NLS-cargo does not impact on Kapβ1–FG Nup binding because Kapα mediates their interaction. However, it is possible that very large NLS-cargoes may limit the occupancy of the transport complex within the FG Nups (Vovk et al., 2016).

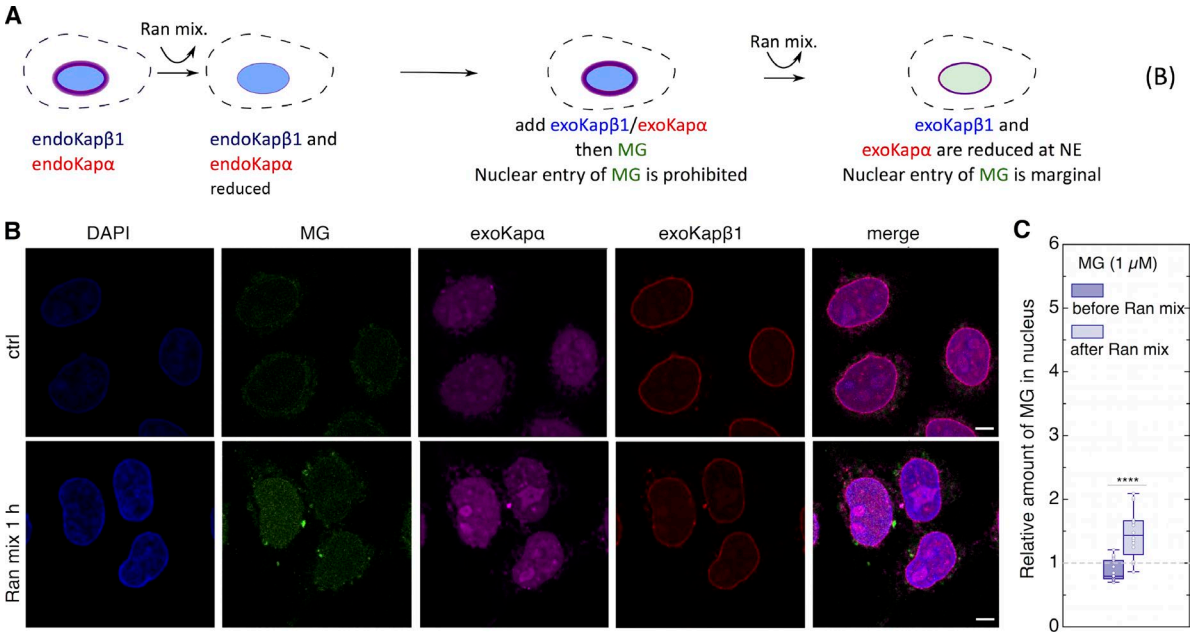

Figure 8. **Kapα-facilitated turnover of Kapβ1 softens the NPC transport barrier against nonspecific cargoes.** (A) Cartoon illustration of the experiment. (B) Kapβ1 turnover is coupled to a softening of the NPC transport barrier with Ran mix–activated transport. (C) Fluorescence quantitation after Ran mix shows that MG entry into the nucleus is marginally increased. $n = 3$ per experimental condition with a total of at least 13 cells being analyzed each. ****, $P < 0.0001$; Student's *t* test. Box plots denote the median, first, and third quartiles. Error bars denote standard deviation, including outliers. Bars, 5 µm.

Quantitative analysis of Kapβ1 turnover in permeabilized cells

Quantitative analysis reveals that the occupancy of each Kapβ1 complex at the NPC depends on its binding affinity with the FG Nups and the extent to which Kapβ1 is depleted by RanGTP (Fig. 4). In turn, the concentration of each molecular partner and its binding isotherm with Kapβ1 will determine the relative amounts of Kapβ1 complexes (Fig. S5). To further validate this, permeabilized cell assays show that RanGTP reduces both Kapα·Kapβ1 (Fig. 5, D and E) and MG-NLS·Kapα·Kapβ1 (Fig. 7, B and C) in a nonmonotonic manner that depends on the concentration of Kapβ1.

Kap-centric versus FG-centric control

Kap-centric control departs from prevailing FG-centric views of the NPC (Fig. 9), which have attempted to explain the form and function of the NPC selective barrier in terms of FG Nup behavior (Rout et al., 2000; Frey and Görlich, 2007; Lim et al., 2007; Yamada et al., 2010). Key evidence for Kap-centric control lies with the NE retention of an endogenous pool of Kapα·Kapβ1 in permeabilized cells (Fig. 5 B), which had not been accounted for previously. This likely represents the physiological steady-state population of endoKapα·Kapβ1 at the NPC that reinforces the NPC barrier (Fig. 6 B). Interestingly, the unobstructed permeation of MG and MG-NLS into the nucleus (Fig. 6 C) was contingent on the removal of endoKapα·Kapβ1 by Ran mix (Fig. 5 B). Still more remarkable is that adding back exoKapβ1 restored barrier function against these substrates (Fig. 6, D–F). Thus, the FG Nups are necessary (to bind Kaps) but insufficient for establishing NPC barrier function. This might explain why FG repeat deletions did not have any significant impact on NPC permeability (Strawn et al., 2004).

As we have shown, the process of selective cargo transport is facilitated in a Kap concentration-dependent manner that determines the overall occupancy of Kap–cargo complexes in the NPC. This is most likely facilitated by the highly flexible and dynamic FG Nups (Sakiyama et al., 2016) that would be able to respond and adapt to local changes in the pore. We postulate that strongly bound Kaps saturate the FG Nups to allow a weakly bound pool to pass (Kapinos et al., 2014), which is consistent with Yang and Musser (2006), who showed that higher Kap concentrations promoted higher transport efficiencies and faster transport times. Indeed, Fig. 7 E shows that the passive entry of MG-NLS into the nucleus increases with increasing exoKapβ1 (and exoKapα) concentrations. In marked contrast, any passive uptake of nonspecific MG cargoes remains blocked (Fig. 8 B; compare with Fig. 6, C and E). Hence, Kap-centric control encapsulates both NPC barrier and selective transport characteristics.

Although RanGTP binds Kapβ1 to release Kapα and NLS-cargoes from the NPC, it is less clear how RanGTP·Kapβ1 returns to the cytoplasm. If RanGTP also dissociates Kapβ1 from the FG Nups (Rexach and Blobel, 1995), RanGTP·Kapβ1 would itself resemble a large nonspecific cargo in the absence of FG Nup binding that contradicts the selective transport criteria. To retain its specificity to the FG Nups, we find that the action of RanGTP subtly switches the high-affinity binding state of MG-NLS·Kapα·Kapβ1 to the lower binding state of RanGTP·Kapβ1 to enable Kapβ1 turnover. Importantly, this is directly correlated to the concomitant release of Kapα (Fig. 5, D and F; and Fig. 7 D) and the nuclear accumulation of MG-NLS (Fig. 7, B–E). On this basis, RanGTP·Kapβ1 efflux is still specific in nature.

Implications of Kap-centric control

A key attribute of Kap-centric control may be to regulate the Ran gradient (Görlich et al., 2003; Riddick and Macara, 2005; Kopito and Elbaum, 2009). Because of its higher affinity for Kapβ1, RanGTP likely outcompetes Kapα for Kapβ1 within the nucleus. This prevents it from traversing further into the NPC

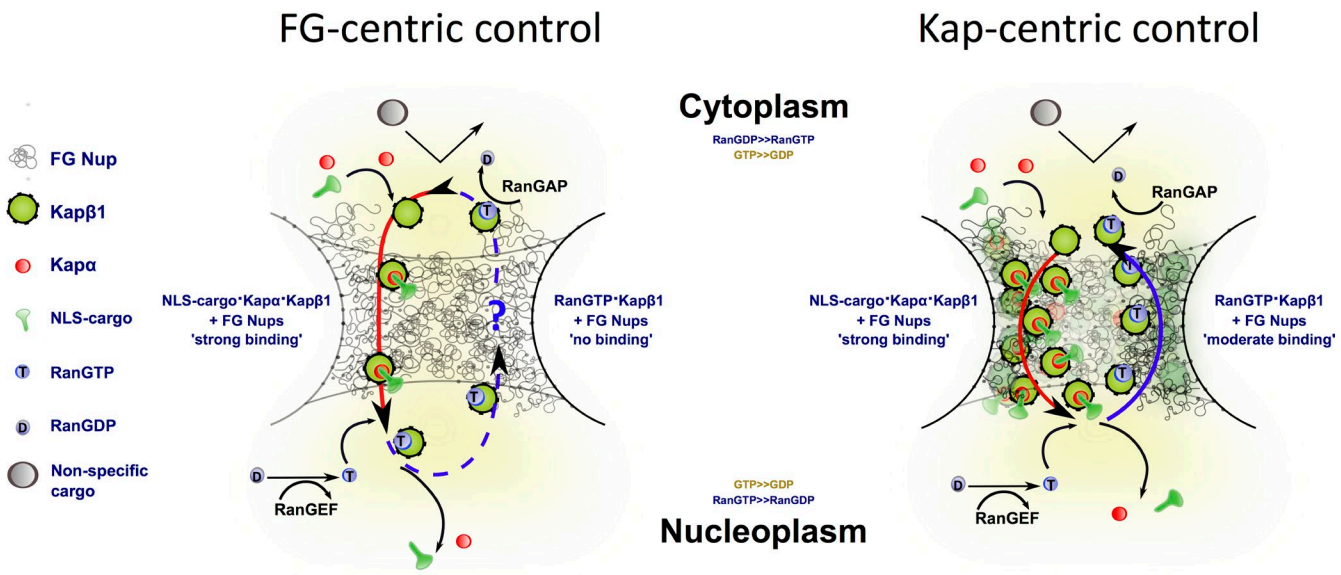

Figure 9. **FG-centric versus Kap-centric NPC transport models.** (Left) FG-centric models explain that an FG Nup barrier regulates selective transport through the NPC without invoking Kap occupancy. (Right) Kap-centric control argues that NPC barrier and transport function is regulated by Kaps in the pore. This is mediated by Kapα, which promotes NLS-cargo·Kapα·Kapβ1 import by switching the transport complex into a high-affinity FG Nup binding state. Upon reaching the nucleus, RanGTP switches Kapβ1 back to its lower affinity state while concomitantly releasing NLS-cargo and Kapα. At steady state, RanGTP·Kapβ1 export is sustained because it does not cross react with Kapα·Kapβ1 within the NPC. The model is constructed according to the equilibrium dissociation constants summarized in Table S4.

on its own, which might explain why RanGTP·Kapβ1 complex formation only occurs at the nuclear basket (Lowe et al., 2015). Upon reaching the cytoplasmic periphery, the chemical potential established by RanGAP (RanGTPase-activating protein) to hydrolyze GTP into GDP (Bischoff et al., 1994) followed by the release of RanGDP from Kapβ1 is what sustains RanGTP·Kapβ1 export (Moroianu and Blobel, 1995). To further underscore the importance of Kapα, we postulate that Kapα·Kapβ1 also helps to outcompete and release RanGTP·Kapβ1 from the FG Nups there. Then, after GTP hydrolysis, the higher affinity of RanGDP toward NTF2 in comparison with Kapβ1 (Chaillan-Huntington et al., 2000; Forwood et al., 2008; Lonhienne et al., 2009) (Table S4) ensures that predominantly RanGDP·NTF2 complexes form in the cytoplasm for import into the nucleus.

Still, 19 other members consisting of importins and exportins exist in the Kapβ family that bind signal-specific cargoes directly (Chook and Süel, 2011; Kimura et al., 2017). Although it remains to be ascertained if and how they contribute to Kap-centric control, IBB-cargo such as SREBP2 (Lee et al., 2003) that binds Kapβ1 directly may provide a good starting point to explore the role of Kapα-independent pathways.

Conclusion

Our work reveals how NPC function is controlled by karyopherins that shuttle cargoes between the nucleus and the cytoplasm. This disagrees with the view that the FG Nups regulate the shuttling of karyopherins and their cargoes. To operate the NPC, Kapα mediates Kapβ1 turnover and occupancy in a RanGTP-dependent manner that simultaneously regulates NLS-cargo release and NPC barrier function. Thus, a deregulation of Kap-centric control could lead to a malfunction in NCT and disease (Kau et al., 2004).

Materials and methods

FG Nup expression and purification

Cysteine-tagged FG domains of four human nucleoporins, Nup62, Nup214, Nup98, and Nup153, were cloned, expressed, and purified as described previously (Kapinos et al., 2014). All proteins were dialyzed into the appropriate buffer (see below) before experimentation. The concentration of these proteins was determined using UV measurements or Bradford assay.

WT Ran and RanQ69L expression, purification, and loading with GTP or GDP

A plasmid (pQE32) with a full-length human RanQ69L construct (the nonhydrolyzing mutant of Ran) was a gift from U. Kutay (ETH Zurich, Zurich, Switzerland) (Kutay et al., 1997b). A WT Ran construct was derived from the aforementioned plasmid using site-directed mutagenesis (primers 5′-GTATGGGACACAGCCGGCCAGGAGAAA TTCGGTGGACTG-3′ and 5′-CAGTCCACCGAATTTCTCCTGGCC GGCTGTGTCCCATAC-3′). His-tagged Ran WT and RanQ69L full-length proteins were induced by 0.5 M IPTG and expressed in BL21 competent cells at 24°C overnight. The cells were lysed for 1 h at 4°C using the following buffer: 50 mM Hepes-KOH, pH 7, 100 mM NaCl, 5 mM DTT, 5 mM $MgCl_2$, and 20 mM imidazole with addition of 40 µl DNase (10 mg/ml), Pefobloc, and lysozyme. Finally, Ran WT and RanQ69L were purified using a nickel–nitrilotriacetic acid (Ni-NTA) column (Roche) in an imidazole gradient (10–500 mM). The purified protein was dialyzed into 10 mM Hepes buffer, pH 7.2, with 100 mM NaCl. Then, Ran WT and RanQ69L were incubated for 30 min at 4°C with 10 mM EDTA and 1 mM GTP or GDP nucleotides. Consequently, 25 mM of excess $MgCl_2$ was added to ensure $MgCl_2$ and GTP (or GDP) binding to nucleotide-free Ran. Finally, Ran WT and RanQ69L loaded with GTP was dialyzed into PBS buffer, pH 7.2 (GIBCO by Life Sciences), in the presence of 1 mM $MgCl_2$ and isolated using an Åkta Purifier on a column (Superdex 200 HiLoad 16/60; GE

Healthcare). Protein purity was analyzed by 12% PAGE at 0.1% SDS (Fig. S2), and Ran WT and RanQ69L concentrations were determined by absorption measurements at 280 nm and correcting it for the GTP or GDP absorption within this region.

Kapβ1 and Kapα expression and purification

Full-length human Kapβ1 was cloned, expressed, and purified as described previously (Kapinos et al., 2014). The plasmid (pQE70) containing a full-length *Xenopus laevis* Kapα construct was a gift from U. Kutay. A full-length human Kapα construct (Addgene template pCMVTNT-T7-KPNA2; plasmid 26678) was cloned into the same pQE70 vector using EcoRI–BamII restriction enzymes. Both constructs have a His_6 tag at its C terminus with a short linker (-GSRSHHHHHH) that does not affect the complex formation of this protein with Kapβ1. Kapα was subsequently purified using an Ni-NTA column (Roche). Finally, Kapα monomers were separated and isolated using a Superdex 200 column, and the collected fractions were stored at −80°C. The final purity of the His_6-tagged Kapα and Kapβ1 was analyzed by 12% PAGE at 0.1% SDS (Fig. S2), and their concentration was determined by absorption measurements at 280 nm.

MG and MG-NLS expression and purification

Sequences of MG-NLS and MG (maltose-binding protein modified at its C terminus with GFP with and without an NLS sequence, respectively) were cloned into pPEP-TEV vector using Sac1–Kpn1 restriction enzymes. The template plasmid containing MG sequence was a gift from L.M. Veenhoff (University Medical Center Groningen, Groningen, Netherlands). The expression and purification of these constructs were done as described for Kapβ1. The N-terminal His_6-tagged proteins were purified using a Ni-NTA column (Roche) and then were separated and isolated using a Superdex 200 column, and the collected fractions were stored at −80°C. The quality and quantity of MG-NLS or MG were verified using 12% SDS-PAGE.

Dynamic light scattering

The hydrodynamic radii of the purified proteins were measured by dynamic light scattering (Zetasizer Nano) as previously described (Kapinos et al., 2014). See Table S1 for details.

ITC

The equilibrium binding constants of RanGTP·Kapβ1 and Kapα·Kapβ1 were measured using a microcalorimeter (VP-ITC; MicroCal, LLC; Fig. S2). All measurements were done at 25°C in a buffer of 20 mM Tris-HCL, pH 7.5, 200 mM NaCl, 1 mM Tris(2-carboxyethyl)phosphine, and 1 mM $MgCl_2$. To measure RanGTP·Kapβ1 complex formation, 21 µM RanGTP was titrated into 3 µM Kapβ1 in the measurement cell (30 injections). To measure Kapα·Kapβ1 complex formation, 49 µM Kapα was titrated into 6 µM Kapβ1 in the measurement cell (30 injections).

MST

The equilibrium dissociation constant of Alexa Fluor 488–Kapα·Kapβ1 was measured in PBS, pH 7.2, at 25°C using a microscale electrophoresis instrument (Monolith NT.115; Nano Temper Technologies; Fig. S2 D). Kapβ1 was mixed with the Alexa Fluor 488–Kapα and placed into capillaries (16 samples; 50 nM Alexa Flour 488–labeled Kapα mixed with 11.4 nM to 5 µM Kapβ1). The equilibrium dissociation constant of MG-NLS with the Kapα·Kapβ1 complex was measured in the same manner (Fig. S2). Kapα·Kapβ1 was mixed with MG-NLS and placed into capillaries (16 samples; 50 nM MG-NLS mixed with 0.06 nM to 4 µM Kapβ1 and 0.12 nM to 8 µM Kapα).

CD

The CD spectra of 5 µM Kapα, 5 µM Kapβ1, and 2.5 µM Kapα·Kapβ1 complexes were measured in 10-mm quartz cuvettes using a CD spectrometer (Chirascan; Applied Photophysics; Fig. S2) in PBS, pH 7.2.

SPR measurements

All SPR measurements were performed at 25°C in PBS, pH 7.2 (GIB CO by Life Technologies), with 1 mM $MgCl_2$ in a four flow cell instrument (Biacore T100; GE Healthcare) as described previously (Schoch et al., 2012; Kapinos et al., 2014). In brief, $C_{17}H_{36}O_4S$ (hydroxyl-terminated tri[ethylene glycol] undecane thiol, HS-$[CH_2]$-$[OCH_2CH_2]_3$-OH, abbreviated as PUT; Nanoscience) and the cysteine-modified FG Nup domains were semicovalently grafted onto a gold sensor surface via thiol binding in cell 1 (reference) and cell 2 (sample; Fig. S1). 1% (wt/vol) BSA (Sigma-Aldrich) solution was prepared in PBS, pH 7.2. Before experimentation, the proteins were dialyzed into PBS, pH 7.2. Experiments with mixed layers were performed by premixing different FG Nup domains in equimolar ratios before being grafted onto the gold sensor surface. All protein and reagent solutions were centrifuged for 15 min at 16,000 *g* to remove particles and bubbles. Buffer solutions were filtered (0.22 µm) and degassed before use. We note that both RanGTP ($n = 4$) and RanQ69L-GTP ($n = 12$) were used in these experiments. However, both variants gave similar results and are henceforth referred to as RanGTP for brevity.

Kinetic analysis of multivalent interactions

All kinetic analyses were carried out as described previously (Kapinos et al., 2014; Wagner et al., 2015). In brief, a set of 36 × 36 ($k_{on,i}$,$k_{off,i}$) pairs was populated, and their fractional abundance was depicted as color intensity in k_{on} versus K_d and k_{off} versus K_d. Each interaction map averaged over ∼10 individual sensograms. Calculations and visualizations were generated using Matlab (MathWorks) and Python.

Permeabilized cell assays

HeLa cells were washed with transport buffer and then permeabilized with 40 µg/ml digitonin in transport buffer for 5 min as described previously (Adam et al., 1990). After permeabilization, the cells were washed with PBS three times for 5 min each and then incubated with Ran mix for 1 h (2 mM GTP, 0.1 mM ATP, 4 mM creatine phosphate, 20 U/ml creatine kinase, 5 µM RanGDP, 4 µM NTF2, and 1 mM DTT; Lowe et al., 2015). For endogenous Kapα and Kapβ1 detection, cells were fixed with 2% PFA for 15 min and stained with anti-Kapα (Santa Cruz), anti-Kapβ1 (3E9; Abcam), and DAPI (Sigma-Aldrich; Fig. 5 B). For the exogenous Kap repopulation assay, exoKapα was conjugated with Alexa Fluor 488 (Thermo Fisher; degree of labeling [DOL] 1.5) or Alexa Fluor 647 (DOL 1.4), whereas exoKapβ1 was conjugated with Alexa Fluor 568 (DOL 2.89). Either exoKapβ1 or exoKapα·Kapβ1 (preincubated for 30 min at RT) was applied for 1 h at the concentrations specified in the main text. Cells were subsequently treated with transport buffer or Ran mix for 1 h. Subsequently, the cells were fixed and stained with anti-Kapβ1 for endoKapβ1, whereas exoKapβ1 or exo Kapα was detected by Alexa Fluor labeling (Fig. 5, C and D). In this regard, anti-Kapβ1 (3E9) recognizes only endoKapβ1 but not exoKapβ1 according to product-specific information. All other experiments involving MG, MG-NLS, and/or exogenous Kaps were conducted by separating a respective batch of cells into parallel sets after the first Ran mix treatment. This was to facilitate (a) immunostaining of endoKapα and endoKapβ1 in the absence of exoKaps and (b) detection of exoKapα and/or exoKapβ1, MG, and MG-NLS after subsequent Ran mix treatments (i.e., not requiring endoKap staining). To investigate NPC barrier function, the nuclear accumulation of 1 µM MG or 1 µM MG-NLS was first measured in permeabilized cells or Ran mix–treated cells after 1-h

incubation. The cells were then treated with 100 nM exoKapβ1 together with MG-NLS or 100 nM exoKapβ1 followed by MG for another 1 h (Fig. 6 B–D). To test for Kapβ1 turnover, MG-NLS coincubated with either exoKapα·Kapβ1 or exoKapβ1 alone was introduced to Ran mix–treated permeabilized cells followed by a second step (Fig. 7). In comparison, Ran mix–treated permeabilized cells were sequentially treated with exoKapα·Kapβ1 and then MG or MG and Ran mix together to check whether the NPC barrier softened during Kapβ1 turnover (Fig. 8). In all cases, cells were then fixed and stained with DAPI.

Fluorescence image analysis

Fluorescence images were obtained at RT with Zen 2010 software using an LSM700 upright confocal microscope (Zeiss) with an oil-immersed 63×/1.4 NA PLAN APO objective and two photomultiplier tube detectors (Hamamatsu). Nuclear rim staining quantification was performed using ImageJ software (National Institutes of Health). Raw data for both DAPI and Kapβ1 channels were first duplicated. The nuclear rim of each permeabilized cell was then defined as a region of interest by converting the DAPI channel into a binary image, followed by the processes of (a) filling holes (to fill up the whole nucleus), (b) outlining (to obtain the nuclear rim outline), and (3) dilating (to generate an ∼700-nm width for the nuclear rim). This region of interest was then applied to measure the mean fluorescence intensity of endoKapβ1 or exoKapβ1 in the Kapβ1 channel as well as in the Kapα channel. The intensity of Ran mix–treated samples was normalized to transport buffer–treated control samples. The mean fluorescence intensity of MG-NLS or MG was measured from the nuclear region defined by the DAPI channel. Similarly, the intensity was normalized to the control samples. Analyzed cell numbers are specified in respective figure legends.

Online supplemental material

Fig. S1 explains the SPR experimental procedure. Fig. S2 presents a summary of ITC, MST, SDS-PAGE, and CD characterization of Kapβ1 and its related complexes in solution. Fig. S3 shows SPR measurements that compare and contrast the effect of RanGTP on the binding of MG-NLS·Kapα·Kapβ1 and standalone Kapβ1 complexes to cNup153, as well as the promiscuous FG Nup binding of RanGTP·Kapβ1 and Kapα·Kapβ1. Fig. S4 shows equilibrium Langmuir isotherm and kinetic analysis of standalone Kapβ1, RanGTP·Kapβ1, Kapα·Kapβ1, and MG-NLS·Kapα·Kapβ1 binding to cNup153, cNup62, cNup214, and cNup98, respectively. Fig. S5 summarizes the quantitative binding analysis by equilibrium calculations and SPR at different mixing ratios and concentrations. Table S1 shows the hydrodynamic diameters of the relevant proteins and transport complexes as determined by dynamic light scattering. Table S2 summarizes Student's *t* test results that validate the significance of the observed differences indicated in the box plots of Fig. 3. Table S3 summarizes Student's *t* test results that validate the significance of the observed differences indicated in the box plots of Figs. 5, 6, 7, and 8. Table S4 provides a comprehensive summary of all complex interactions and their equilibrium dissociation constants.

Acknowledgments

We acknowledge in-house facility support at the Biozentrum. In particular, we thank T. Sharpe from the Biophysics Core Facility and various members of the Imaging Core Facility for assistance and advice.

This work was supported by the Swiss National Science Foundation (grant 31003A_146612), the Biozentrum at the University of Basel, and the Swiss Nanoscience Institute.

The authors declare no competing financial interests.

Author contributions: L.E. Kapinos, B. Huang, and R.Y.H. Lim conceived and designed the study. L.E. Kapinos performed all biophysical experiments and quantitative analysis. B. Huang carried out all permeabilized cell assays, including confocal microscopy and image analysis. C. Rencurel cloned, expressed, and purified proteins. R.Y.H. Lim wrote the paper together with L.E. Kapinos and B. Huang. All authors discussed the results and commented on the manuscript.

Submitted: 15 February 2017
Revised: 16 June 2017
Accepted: 8 August 2017

References

Adam, S.A., R.S. Marr, and L. Gerace. 1990. Nuclear protein import in permeabilized mammalian cells requires soluble cytoplasmic factors. *J. Cell Biol.* 111:807–816. http://dx.doi.org/10.1083/jcb.111.3.807

Allen, N.P., L. Huang, A. Burlingame, and M. Rexach. 2001. Proteomic analysis of nucleoporin interacting proteins. *J. Biol. Chem.* 276:29268–29274. http://dx.doi.org/10.1074/jbc.M102629200

Bayliss, R., T. Littlewood, and M. Stewart. 2000. Structural basis for the interaction between FxFG nucleoporin repeats and importin-β in nuclear trafficking. *Cell.* 102:99–108. http://dx.doi.org/10.1016/S0092-8674(00)00014-3

Bednenko, J., G. Cingolani, and L. Gerace. 2003. Importin β contains a COOH-terminal nucleoporin binding region important for nuclear transport. *J. Cell Biol.* 162:391–401. http://dx.doi.org/10.1083/jcb.200303085

Ben-Efraim, I., and L. Gerace. 2001. Gradient of increasing affinity of importin β for nucleoporins along the pathway of nuclear import. *J. Cell Biol.* 152:411–417. http://dx.doi.org/10.1083/jcb.152.2.411

Bischoff, F.R., C. Klebe, J. Kretschmer, A. Wittinghofer, and H. Ponstingl. 1994. RanGAP1 induces GTPase activity of nuclear Ras-related Ran. *Proc. Natl. Acad. Sci. USA.* 91:2587–2591. http://dx.doi.org/10.1073/pnas.91.7.2587

Catimel, B., T. Teh, M.R. Fontes, I.G. Jennings, D.A. Jans, G.J. Howlett, E.C. Nice, and B. Kobe. 2001. Biophysical characterization of interactions involving importin-α during nuclear import. *J. Biol. Chem.* 276:34189–34198. http://dx.doi.org/10.1074/jbc.M103531200

Chaillan-Huntington, C., C.V. Braslavsky, J. Kuhlmann, and M. Stewart. 2000. Dissecting the interactions between NTF2, RanGDP, and the nucleoporin XFXFG repeats. *J. Biol. Chem.* 275:5874–5879. http://dx.doi.org/10.1074/jbc.275.8.5874

Chook, Y.M., and K.E. Süel. 2011. Nuclear import by karyopherin-βs: recognition and inhibition. *Biochim. Biophys. Acta.* 1813:1593–1606. http://dx.doi.org/10.1016/j.bbamcr.2010.10.014

Christie, M., C.W. Chang, G. Róna, K.M. Smith, A.G. Stewart, A.A. Takeda, M.R. Fontes, M. Stewart, B.G. Vértessy, J.K. Forwood, and B. Kobe. 2016. Structural biology and regulation of protein import into the nucleus. *J. Mol. Biol.* 428:2060–2090. http://dx.doi.org/10.1016/j.jmb.2015.10.023

Cingolani, G., C. Petosa, K. Weis, and C.W. Müller. 1999. Structure of importin-β bound to the IBB domain of importin-α. *Nature.* 399:221–229. http://dx.doi.org/10.1038/20367

Cingolani, G., H.A. Lashuel, L. Gerace, and C.W. Müller. 2000. Nuclear import factors importin α and importin β undergo mutually induced conformational changes upon association. *FEBS Lett.* 484:291–298. http://dx.doi.org/10.1016/S0014-5793(00)02154-2

Conti, E., C.W. Müller, and M. Stewart. 2006. Karyopherin flexibility in nucleocytoplasmic transport. *Curr. Opin. Struct. Biol.* 16:237–244. http://dx.doi.org/10.1016/j.sbi.2006.03.010

Delphin, C., T. Guan, F. Melchior, and L. Gerace. 1997. RanGTP targets p97 to RanBP2, a filamentous protein localized at the cytoplasmic periphery of the nuclear pore complex. *Mol. Biol. Cell.* 8:2379–2390. http://dx.doi.org/10.1091/mbc.8.12.2379

Eibauer, M., M. Pellanda, Y. Turgay, A. Dubrovsky, A. Wild, and O. Medalia. 2015. Structure and gating of the nuclear pore complex. *Nat. Commun.* 6:7532. http://dx.doi.org/10.1038/ncomms8532

Eisele, N.B., S. Frey, J. Piehler, D. Görlich, and R.P. Richter. 2010. Ultrathin nucleoporin phenylalanine-glycine repeat films and their interaction with nuclear transport receptors. *EMBO Rep.* 11:366–372. http://dx.doi.org/10.1038/embor.2010.34

Falces, J., I. Arregi, P.V. Konarev, M.A. Urbaneja, D.I. Svergun, S.G. Taneva, and S. Bañuelos. 2010. Recognition of nucleoplasmin by its nuclear transport receptor importin α/β: insights into a complete import complex. *Biochemistry.* 49:9756–9769. http://dx.doi.org/10.1021/bi101179g

Floer, M., G. Blobel, and M. Rexach. 1997. Disassembly of RanGTP-karyopherin β complex, an intermediate in nuclear protein import. *J. Biol. Chem.* 272:19538–19546. http://dx.doi.org/10.1074/jbc.272.31.19538

Forwood, J.K., T.G. Lonhienne, M. Marfori, G. Robin, W. Meng, G. Guncar, S.M. Liu, M. Stewart, B.J. Carroll, and B. Kobe. 2008. Kap95p binding induces the switch loops of RanGDP to adopt the GTP-bound conformation: implications for nuclear import complex assembly dynamics. *J. Mol. Biol.* 383:772–782. http://dx.doi.org/10.1016/j.jmb.2008.07.090

Forwood, J.K., A. Lange, U. Zachariae, M. Marfori, C. Preast, H. Grubmüller, M. Stewart, A.H. Corbett, and B. Kobe. 2010. Quantitative structural analysis of importin-β flexibility: paradigm for solenoid protein structures. *Structure.* 18:1171–1183. http://dx.doi.org/10.1016/j.str.2010.06.015

Frey, S., and D. Görlich. 2007. A saturated FG-repeat hydrogel can reproduce the permeability properties of nuclear pore complexes. *Cell.* 130:512–523. http://dx.doi.org/10.1016/j.cell.2007.06.024

Fukuhara, N., E. Fernandez, J. Ebert, E. Conti, and D. Svergun. 2004. Conformational variability of nucleo-cytoplasmic transport factors. *J. Biol. Chem.* 279:2176–2181. http://dx.doi.org/10.1074/jbc.M309112200

Görlich, D., and U. Kutay. 1999. Transport between the cell nucleus and the cytoplasm. *Annu. Rev. Cell Dev. Biol.* 15:607–660. http://dx.doi.org/10.1146/annurev.cellbio.15.1.607

Görlich, D., F. Vogel, A.D. Mills, E. Hartmann, and R.A. Laskey. 1995. Distinct functions for the two importin subunits in nuclear protein import. *Nature.* 377:246–248. http://dx.doi.org/10.1038/377246a0

Görlich, D., N. Panté, U. Kutay, U. Aebi, and F.R. Bischoff. 1996. Identification of different roles for RanGDP and RanGTP in nuclear protein import. *EMBO J.* 15:5584–5594.

Görlich, D., M.J. Seewald, and K. Ribbeck. 2003. Characterization of Ran-driven cargo transport and the RanGTPase system by kinetic measurements and computer simulation. *EMBO J.* 22:1088–1100. http://dx.doi.org/10.1093/emboj/cdg113

Grünwald, D., and R.H. Singer. 2010. In vivo imaging of labelled endogenous β-actin mRNA during nucleocytoplasmic transport. *Nature.* 467:604–607. http://dx.doi.org/10.1038/nature09438

Hahn, S., and G. Schlenstedt. 2011. Importin β-type nuclear transport receptors have distinct binding affinities for Ran-GTP. *Biochem. Biophys. Res. Commun.* 406:383–388. http://dx.doi.org/10.1016/j.bbrc.2011.02.051

Halder, K., N. Dölker, Q. Van, I. Gregor, A. Dickmanns, I. Baade, R.H. Kehlenbach, R. Ficner, J. Enderlein, H. Grubmüller, and H. Neumann. 2015. MD simulations and FRET reveal an environment-sensitive conformational plasticity of importin-β. *Biophys. J.* 109:277–286. http://dx.doi.org/10.1016/j.bpj.2015.06.014

Hough, L.E., K. Dutta, S. Sparks, D.B. Temel, A. Kamal, J. Tetenbaum-Novatt, M.P. Rout, and D. Cowburn. 2015. The molecular mechanism of nuclear transport revealed by atomic-scale measurements. *eLife.* 4:e10027. http://dx.doi.org/10.7554/eLife.10027

Isgro, T.A., and K. Schulten. 2005. Binding dynamics of isolated nucleoporin repeat regions to importin-β. *Structure.* 13:1869–1879. http://dx.doi.org/10.1016/j.str.2005.09.007

Kapinos, L.E., R.L. Schoch, R.S. Wagner, K.D. Schleicher, and R.Y.H. Lim. 2014. Karyopherin-centric control of nuclear pores based on molecular occupancy and kinetic analysis of multivalent binding with FG nucleoporins. *Biophys. J.* 106:1751–1762. http://dx.doi.org/10.1016/j.bpj.2014.02.021

Kau, T.R., J.C. Way, and P.A. Silver. 2004. Nuclear transport and cancer: from mechanism to intervention. *Nat. Rev. Cancer*. 4:106–117. http://dx.doi.org/10.1038/nrc1274

Kimura, M., Y. Morinaka, K. Imai, S. Kose, P. Horton, and N. Imamoto. 2017. Extensive cargo identification reveals distinct biological roles of the 12 importin pathways. *eLife.* 6:e21184. http://dx.doi.org/10.7554/eLife.21184

Kopito, R.B., and M. Elbaum. 2009. Nucleocytoplasmic transport: a thermodynamic mechanism. *HFSP J.* 3:130–141. http://dx.doi.org/10.2976/1.3080807

Kubitscheck, U., D. Grünwald, A. Hoekstra, D. Rohleder, T. Kues, J.P. Siebrasse, and R. Peters. 2005. Nuclear transport of single molecules: dwell times at the nuclear pore complex. *J. Cell Biol.* 168:233–243. http://dx.doi.org/10.1083/jcb.200411005

Kutay, U., F.R. Bischoff, S. Kostka, R. Kraft, and D. Görlich. 1997a. Export of importin α from the nucleus is mediated by a specific nuclear transport factor. *Cell.* 90:1061–1071. http://dx.doi.org/10.1016/S0092-8674(00)80372-4

Kutay, U., E. Izaurralde, F.R. Bischoff, I.W. Mattaj, and D. Görlich. 1997b. Dominant-negative mutants of importin-β block multiple pathways of import and export through the nuclear pore complex. *EMBO J.* 16:1153–1163. http://dx.doi.org/10.1093/emboj/16.6.1153

Lee, S.J., T. Sekimoto, E. Yamashita, E. Nagoshi, A. Nakagawa, N. Imamoto, M. Yoshimura, H. Sakai, K.T. Chong, T. Tsukihara, and Y. Yoneda. 2003. The structure of importin-β bound to SREBP-2: nuclear import of a transcription factor. *Science.* 302:1571–1575. http://dx.doi.org/10.1126/science.1088372

Lee, S.J., Y. Matsuura, S.M. Liu, and M. Stewart. 2005. Structural basis for nuclear import complex dissociation by RanGTP. *Nature.* 435:693–696. http://dx.doi.org/10.1038/nature03578

Lim, R.Y.H., B. Fahrenkrog, J. Köser, K. Schwarz-Herion, J. Deng, and U. Aebi. 2007. Nanomechanical basis of selective gating by the nuclear pore complex. *Science.* 318:640–643. http://dx.doi.org/10.1126/science.1145980

Lim, R.Y.H., B. Huang, and L.E. Kapinos. 2015. How to operate a nuclear pore complex by Kap-centric control. *Nucleus.* 6:366–372. http://dx.doi.org/10.1080/19491034.2015.1090061

Lolodi, O., H. Yamazaki, S. Otsuka, M. Kumeta, and S.H. Yoshimura. 2016. Dissecting in vivo steady-state dynamics of karyopherin-dependent nuclear transport. *Mol. Biol. Cell.* 27:167–176. http://dx.doi.org/10.1091/mbc.E15-08-0601

Lonhienne, T.G., J.K. Forwood, M. Marfori, G. Robin, B. Kobe, and B.J. Carroll. 2009. Importin-β is a GDP-to-GTP exchange factor of Ran: implications for the mechanism of nuclear import. *J. Biol. Chem.* 284:22549–22558. http://dx.doi.org/10.1074/jbc.M109.019935

Lowe, A.R., J.H. Tang, J. Yassif, M. Graf, W.Y. Huang, J.T. Groves, K. Weis, and J.T. Liphardt. 2015. Importin-β modulates the permeability of the nuclear pore complex in a Ran-dependent manner. *eLife.* 4. http://dx.doi.org/10.7554/eLife.04052

Lyman, S.K., T. Guan, J. Bednenko, H. Wodrich, and L. Gerace. 2002. Influence of cargo size on Ran and energy requirements for nuclear protein import. *J. Cell Biol.* 159:55–67. http://dx.doi.org/10.1083/jcb.200204163

Makise, M., D.R. Mackay, S. Elgort, S.S. Shankaran, S.A. Adam, and K.S. Ullman. 2012. The Nup153-Nup50 protein interface and its role in nuclear import. *J. Biol. Chem.* 287:38515–38522. http://dx.doi.org/10.1074/jbc.M112.378893

Milles, S., D. Mercadante, I.V. Aramburu, M.R. Jensen, N. Banterle, C. Koehler, S. Tyagi, J. Clarke, S.L. Shammas, M. Blackledge, et al. 2015. Plasticity of an ultrafast interaction between nucleoporins and nuclear transport receptors. *Cell.* 163:734–745. http://dx.doi.org/10.1016/j.cell.2015.09.047

Moroianu, J., and G. Blobel. 1995. Protein export from the nucleus requires the GTPase Ran and GTP hydrolysis. *Proc. Natl. Acad. Sci. USA.* 92:4318–4322. http://dx.doi.org/10.1073/pnas.92.10.4318

Moroianu, J., G. Blobel, and A. Radu. 1995. Previously identified protein of uncertain function is karyopherin alpha and together with karyopherin beta docks import substrate at nuclear pore complexes. *Proc. Natl. Acad. Sci. USA.* 92:2008–2011. http://dx.doi.org/10.1073/pnas.92.6.2008

Nigg, E.A. 1997. Nucleocytoplasmic transport: signals, mechanisms and regulation. *Nature.* 386:779–787. http://dx.doi.org/10.1038/386779a0

Ogawa, Y., Y. Miyamoto, M. Oka, and Y. Yoneda. 2012. The interaction between importin-α and Nup153 promotes importin-α/β-mediated nuclear import. *Traffic.* 13:934–946. http://dx.doi.org/10.1111/j.1600-0854.2012.01367.x

Paradise, A., M.K. Levin, G. Korza, and J.H. Carson. 2007. Significant proportions of nuclear transport proteins with reduced intracellular mobilities resolved by fluorescence correlation spectroscopy. *J. Mol. Biol.* 365:50–65. http://dx.doi.org/10.1016/j.jmb.2006.09.089

Popken, P., A. Ghavami, P.R. Onck, B. Poolman, and L.M. Veenhoff. 2015. Size-dependent leak of soluble and membrane proteins through the yeast nuclear pore complex. *Mol. Biol. Cell.* 26:1386–1394. http://dx.doi.org/10.1091/mbc.E14-07-1175

Pumroy, R.A., and G. Cingolani. 2015. Diversification of importin-α isoforms in cellular trafficking and disease states. *Biochem. J.* 466:13–28. http://dx.doi.org/10.1042/BJ20141186

Pyhtila, B., and M. Rexach. 2003. A gradient of affinity for the karyopherin Kap95p along the yeast nuclear pore complex. *J. Biol. Chem.* 278:42699–42709. http://dx.doi.org/10.1074/jbc.M307135200

Rexach, M., and G. Blobel. 1995. Protein import into nuclei: association and dissociation reactions involving transport substrate, transport factors, and nucleoporins. *Cell.* 83:683–692. http://dx.doi.org/10.1016/0092-8674(95)90181-7

Ribbeck, K., G. Lipowsky, H.M. Kent, M. Stewart, and D. Görlich. 1998. NTF2 mediates nuclear import of Ran. *EMBO J.* 17:6587–6598. http://dx.doi.org/10.1093/emboj/17.22.6587

Riddick, G., and I.G. Macara. 2005. A systems analysis of importin-α–β mediated nuclear protein import. *J. Cell Biol.* 168:1027–1038. http://dx.doi.org/10.1083/jcb.200409024

Rout, M.P., J.D. Aitchison, A. Suprapto, K. Hjertaas, Y. Zhao, and B.T. Chait. 2000. The yeast nuclear pore complex: composition, architecture, and transport mechanism. *J. Cell Biol.* 148:635–651. http://dx.doi.org/10.1083/jcb.148.4.635

Sakiyama, Y., A. Mazur, L.E. Kapinos, and R.Y.H. Lim. 2016. Spatiotemporal dynamics of the nuclear pore complex transport barrier resolved by high-speed atomic force microscopy. *Nat. Nanotechnol.* 11:719–723. http://dx.doi.org/10.1038/nnano.2016.62

Schoch, R.L., L.E. Kapinos, and R.Y.H. Lim. 2012. Nuclear transport receptor binding avidity triggers a self-healing collapse transition in FG-nucleoporin molecular brushes. *Proc. Natl. Acad. Sci. USA.* 109:16911–16916. http://dx.doi.org/10.1073/pnas.1208440109

Stewart, M. 2007. Molecular mechanism of the nuclear protein import cycle. *Nat. Rev. Mol. Cell Biol.* 8:195–208. http://dx.doi.org/10.1038/nrm2114

Strawn, L.A., T. Shen, N. Shulga, D.S. Goldfarb, and S.R. Wente. 2004. Minimal nuclear pore complexes define FG repeat domains essential for transport. *Nat. Cell Biol.* 6:197–206. http://dx.doi.org/10.1038/ncb1097

Sun, C., G. Fu, D. Ciziene, M. Stewart, and S.M. Musser. 2013. Choreography of importin-α/CAS complex assembly and disassembly at nuclear pores. *Proc. Natl. Acad. Sci. USA.* 110:E1584–E1593. http://dx.doi.org/10.1073/pnas.1220610110

Tauchert, M.J., C. Hémonnot, P. Neumann, S. Köster, R. Ficner, and A. Dickmanns. 2016. Impact of the crystallization condition on importin-β conformation. *Acta Crystallogr. D Struct. Biol.* 72:705–717. http://dx.doi.org/10.1107/S2059798316004940

Timney, B.L., B. Raveh, R. Mironska, J.M. Trivedi, S.J. Kim, D. Russel, S.R. Wente, A. Sali, and M.P. Rout. 2016. Simple rules for passive diffusion through the nuclear pore complex. *J. Cell Biol.* 215:57–76. http://dx.doi.org/10.1083/jcb.201601004

Tokunaga, M., N. Imamoto, and K. Sakata-Sogawa. 2008. Highly inclined thin illumination enables clear single-molecule imaging in cells. *Nat. Methods.* 5:159–161. http://dx.doi.org/10.1038/nmeth1171

Tu, L.C., G. Fu, A. Zilman, and S.M. Musser. 2013. Large cargo transport by nuclear pores: implications for the spatial organization of FG-nucleoporins. *EMBO J.* 32:3220–3230. http://dx.doi.org/10.1038/emboj.2013.239

von Appen, A., J. Kosinski, L. Sparks, A. Ori, A.L. DiGuilio, B. Vollmer, M.T. Mackmull, N. Banterle, L. Parca, P. Kastritis, et al. 2015. In situ structural analysis of the human nuclear pore complex. *Nature.* 526:140–143. http://dx.doi.org/10.1038/nature15381

Vovk, A., C. Gu, M.G. Opferman, L.E. Kapinos, R.Y.H. Lim, R.D. Coalson, D. Jasnow, and A. Zilman. 2016. Simple biophysics underpins collective conformations of the intrinsically disordered proteins of the nuclear pore complex. *eLife*. 5:5. http://dx.doi.org/10.7554/eLife.10785

Wagner, R.S., L.E. Kapinos, N.J. Marshall, M. Stewart, and R.Y.H. Lim. 2015. Promiscuous binding of Karyopherinβ1 modulates FG nucleoporin barrier function and expedites NTF2 transport kinetics. *Biophys. J.* 108:918–927. http://dx.doi.org/10.1016/j.bpj.2014.12.041

Weis, K., C. Dingwall, and A.I. Lamond. 1996. Characterization of the nuclear protein import mechanism using Ran mutants with altered nucleotide binding specificities. *EMBO J.* 15:7120–7128.

Yamada, J., J.L. Phillips, S. Patel, G. Goldfien, A. Calestagne-Morelli, H. Huang, R. Reza, J. Acheson, V.V. Krishnan, S. Newsam, et al. 2010. A bimodal distribution of two distinct categories of intrinsically disordered structures with separate functions in FG nucleoporins. *Mol. Cell. Proteomics.* 9:2205–2224. http://dx.doi.org/10.1074/mcp.M000035-MCP201

Yang, W., and S.M. Musser. 2006. Nuclear import time and transport efficiency depend on importin β concentration. *J. Cell Biol.* 174:951–961. http://dx.doi.org/10.1083/jcb.200605053

Yang, W., J. Gelles, and S.M. Musser. 2004. Imaging of single-molecule translocation through nuclear pore complexes. *Proc. Natl. Acad. Sci. USA.* 101:12887–12892. http://dx.doi.org/10.1073/pnas.0403675101

Yoshimura, S.H., M. Kumeta, and K. Takeyasu. 2014. Structural mechanism of nuclear transport mediated by importin β and flexible amphiphilic proteins. *Structure.* 22:1699–1710. http://dx.doi.org/10.1016/j.str.2014.10.009

Zachariae, U., and H. Grubmüller. 2008. Importin-β: structural and dynamic determinants of a molecular spring. *Structure.* 16:906–915. http://dx.doi.org/10.1016/j.str.2008.03.007